Hybrid Adaptive Integrated Chassis Control

vehicle lateral stability in presence of uncertainty

Dhruv Jagga

Master of Science Thesis

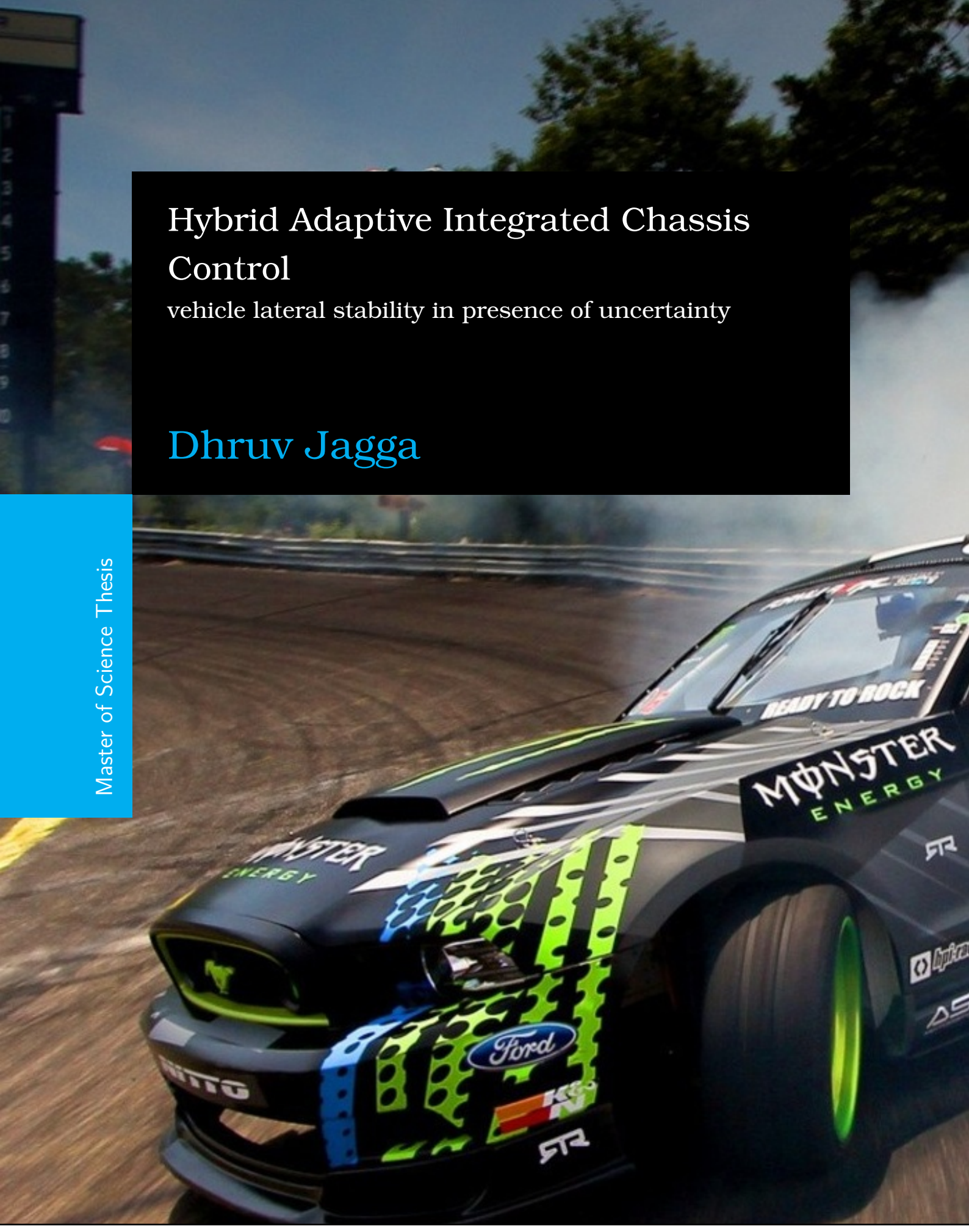

TU Delft Delft University of Technology

Delft Center for Systems and Control

Hybrid Adaptive Integrated Chassis Control

vehicle lateral stability in presence of uncertainty

MASTER OF SCIENCE THESIS

For the degree of Master of Science in Systems and Control at Delft University of Technology

Dhruv Jagga

August 29, 2017

Faculty of Mechanical, Maritime and Materials Engineering · Delft University of Technology

DELFT UNIVERSITY OF TECHNOLOGY
DEPARTMENT OF
DELFT CENTER FOR SYSTEMS AND CONTROL (DCSC)

The undersigned hereby certify that they have read and recommend to the Faculty of Mechanical, Maritime and Materials Engineering for acceptance of a thesis entitled

HYBRID ADAPTIVE INTEGRATED CHASSIS CONTROL

by

DHRUV JAGGA

in partial fulfillment of the requirements for the degree of

MASTER OF SCIENCE SYSTEMS AND CONTROL

Dated: August 29, 2017

Supervisor(s):

dr.ir. Simone. Baldi

Reader(s):

dr.ir.T.J.J. van den Boom

dr.ir. Barys Shyrokau

Mr. Shuai Yuan

Abstract

Extensive advancements in the field of mobility and safety in transportation in last few decades have acted as a catalyst for the expansion of automobile industry. The research for the evolution of new technologies, vehicle safety regulations and specifications and the market requirements has given this progress a greater push. The passenger cars these days are equipped with ample collection of active safety systems such as Anti-lock Braking Systems (ABS), Electronic Stability Program (ESP), Active Front Steering (AFS) and many more. The amalgamation of these active safety systems in the vehicle chassis allows the vehicle to accomplish the desired stability.

Both academia and industry understood the requirement of more research in the field of vehicle industry. This leads to the comprehensive enhancement in the field of research and development with respect to integrated chassis control (ICC). The new research delivered some remarkable advantages to this industry, such as cost reduction of the complete system, multi-objective performance growth, hardware entanglement, fault-tolerant capability and system plausibility.

Despite the huge diversity in research of integrated chassis, there are certain adaptive design methods which can be used to enhance the ICC performance. This dissertation intends to provide a methodology to fully exploit the nonlinear dynamics of the vehicle concerning the forces in between tire and road surface and to discuss the integration of AFS and ESP. It establishes a novel adaptive control approach in order to attain asymptotic tracking for switched affine vehicle models with parameter uncertainties and disturbances acting on the model. This, therefore, will help to attain the desired performance. Further, comparison with strategies that merely exploits the linear region of the vehicle dynamics are discussed, and performance improvements of the proposed methodology are assessed. Finally, analytically the endurance of the prospective control strategy is proven and simulations are conducted to validate the theoretical analysis.

Keywords: Lateral Stability Control, Yaw Stability Control, Vehicle Dynamics, PWA Vehicle Model, Pacejka Magic Formula, Integrated Chassis Control, Hybrid Adaptive Control.

Contents

List of Figures

List of Tables

Acknowledgements

The completion of this challenging project as my master thesis would not have been possible without some external support. I would like to thank all DCSC community people for maintaining a stimulating environment which helps to shape up the overall personality of a student.

I would like to express my deepest gratitude to my supervisor, dr.ir. Simone Baldi for providing me the opportunity to work on such a promising research topic. I would also like to thank him for his continuous support and guidance throughout the project.

I would extend my gratitude to dr.ir. Barys Shyrokau for his invaluable comments at the final stage of the project which helped me to improve my work.

Finally, I would like to express my deepest gratitude and love towards my family and friends for providing unconditional support, love, and having faith in me.

Delft, University of Technology
August 29, 2017

Dhruv Jagga

"The real struggle in life is with ourselves. The true secret of success is the refusal to give up, the refusal to fail; it lies in the struggle to win the battle against one's own weakness."

— *Daisaku Ikeda*

Chapter 1

Introduction

The autonomous driving has become an active area of research with an objective to certify the safety and comfort in driving a vehicle. In order to achieve these objectives, a crucial role is played by the control of vehicle dynamics. Control should make the vehicle effectively follow the actions commanded by the driver in premises of acceleration, braking and cornering. Most of the normal drivers have no idea about the vehicle's handling limit. Or in other words, most people drive vehicle only in linear handling regime. The scheme of linear handling is the subjective view of handling feel by the driver while administering a vehicle. During nonlinear handling conditions in critical maneuvers like high-speed cornering, the vehicle is pushed into the unstable region resulting in large side-slip angle and reaching the tire adhesion limits. These critical maneuvers can be cautiously overturned by using various driver assistance systems (DAS) installed in the vehicle chassis. In recent years, the control engineering has played a crucial role in developing these active chassis control systems. When observed from the handling point of view, these systems aims to improve the vehicle handling by expanding the linear handling region. This results in improving the handling impression during the normal driving and provides stability near the tire limits eventually preventing the occurrence of accidents.

In the early stage of research these active safety systems were used independently or in parallel with one another to attain the vehicle stability [7]. Further, to avoid the increased complexity and to slash the redundancy of the expensive hardware, recent research focuses on the integrated chassis control system. The integrated chassis control (ICC) cannot only stabilize the motion of the vehicle but also optimizes the adhesion properties in between the tire and the road. This prevents the vehicle from reaching the handling limits and also subside the loss over the control of the vehicle.

In order to improve the vehicle dynamical control, the lateral dynamic control in particular and to attain the desired stability by improving the handling performance, the yaw stability control is required as described in Figure 1-1. The yaw stability control also known as directional stability is mostly influenced by steering and braking inputs.

The vehicle traveling on a road can spin and slide if the friction between the tire and the surface of the road is not ample to generate the required lateral force and momentum. This can result in fatal

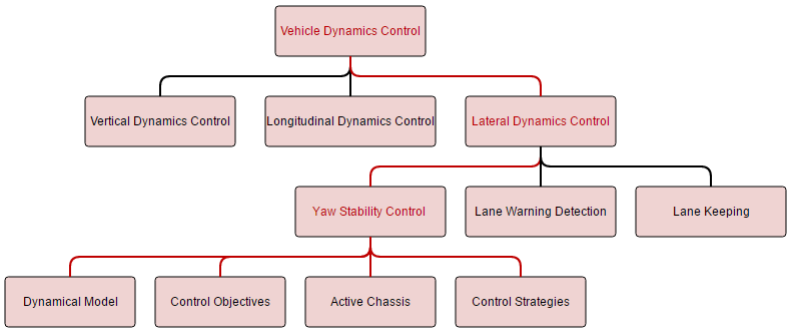

Figure 1-1: Vehicle dynamic control

situations on road. To prevent these situations and to allow the vehicle to follow the intended path safely by the driver, the directional stability is required. This is not possible without the presence of active safety control such as active front steering (AFS), anti-lock braking system (ABS), electronic stability program (ESP) and many more. To achieve the highest potential of these active safety systems, it is required that they work together to achieve the performance objectives. The ICC does this job. The ICC system is able to prevent the conflicts and interventions in between different active safety systems and also provide proper coordination and communication among these subsystems in order to achieve the improved stability of the vehicle. The timeline in Figure 1-2 shows the involvement of these subsystems in the last two decades. It can be seen that with the objective of achieving vehicle stability new active safety systems are continuously incorporated in the ICC design.

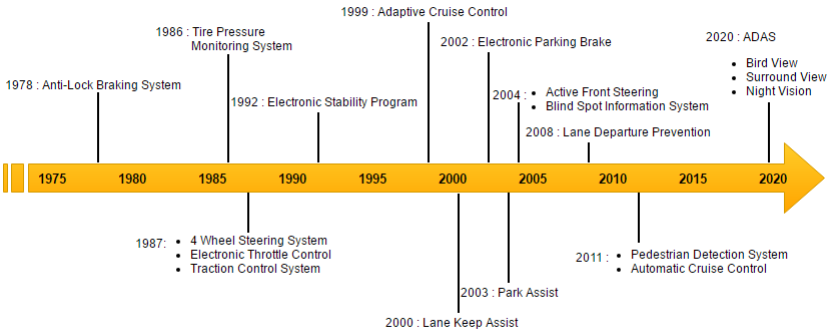

Figure 1-2: Timeline: Integrated Chassis Control subsystems

The AFS and ESP from these are the most important to achieve the lateral dynamic yaw stability for the vehicle and are considered as core features in this particular dissertation.

1-1 State-of-the-art

Control algorithms play a decisive role in managing the dynamics of the vehicle and allow the vehicle to behave in the desired manner. The enormous number of families of control algorithms have been used to tackle the problems arousing in vehicle stability. The usage of the respective

control algorithms directly depend upon the system and the control objectives linked with it. the proposed ICC framework is usually derived from steady state cornering by accessing the independent control inputs, which are front steering angle (δ_f) and yaw moment (ΔM) generated from differential braking [8].

The control algorithms in ICC framework can be classified into the following types:

- Linear control technique.
- Nonlinear control technique.
- Intelligent control technique.
- Optimization control technique.

1-1-1 Linear control technique

All the linear control algorithms perform best with the systems defined by the linear tire characteristics (i.e. preventing the tires to reach their gripping limits) and linear vehicle dynamics assumptions. The feedback and feedforward control laws have been previously employed on the linear system to govern the yaw rate and side slip angle to track the desired response [9]. State feedback design, linear quadratic regulator (LQR), pole-placement, H_2/LQG or H_∞ techniques were also used in research to attain the yaw stability [10]. In order to prevent the vehicle from spinning and to improve the cornering performance, the linear robust H_∞ controller was proposed [11]. Shim $et\ al.$ [12] used sliding mode control to attain the effective controller design to cater matched and mismatched disturbances and uncertainties for the stability of vehicle model.

1-1-2 Nonlinear control technique

The drawbacks and the insufficient performance of linear control algorithms have spurred great advances in research and application of the nonlinear control algorithms. For integrated steering and braking systems, feedback linearization was proposed which aims to cancel out the nonlinearities from nonlinear system and linearizes the control-loop dynamics. These algorithms were mostly based on the assumptions in which inverted tire models were considered which might not be applicable in the practical scenario [13].

The active approaches to achieve dynamic yaw stability includes model predictive control (MPC), optimization based control algorithms and adaptive techniques. The model reference adaptive control (MRAC) was used to improve the driving safety and comfort, regulating the steering command depending upon the vehicle response [14]. Further, an ICC based upon the direct Lyapunov method was developed to improve vehicle yaw stability [13, 15].

MPC control scheme was used to stabilize the yaw motion of the vehicle by predicting the near future using the vehicle dynamics. Vehicle safety was further enhanced by using the differential braking and active steering to achieve the vehicle lateral and yaw stability [16]. Another approach used the active safety based on the MPC technique which efficiently complemented its passive safety counterparts. This technique focused on the dynamics involved with the longitudinal motion to introduce better braking and traction control [17].

1-1-3 Intelligent control techniques

Most of the research in the field of autonomous driving is based on model-based control techniques. This requires the development of the accurate reference model and the control technique to achieve the desired objectives. If these models are not assumed with precision the poor performance can be expected from the system. Hence, various techniques such as fuzzy logic control, neural network control etc. have become the hot area of research. Tahami *et al*. used the fuzzy logic control to integrate the subsystems AFS and dynamic yaw control (DYC) to achieve the vehicle stability [18]. Many other pieces of research also used the concept of fuzzy logic control as a knowledge based control to mimic the human experience in order to control the complex systems. This technique require less amount of knowledge or information as compared to conventional mathematical models to give the desired performance. In this approach the controller was described in fuzzy linguistic terms which made it challenging to implement especially while tuning the controller using the fuzzy rules.

1-1-4 Optimization based control techniques

Certain modern control designs have been influenced by the control schemes established on optimization algorithms. These mathematical optimization schemes were used in high-level MPC controllers or control allocations (CA). Such algorithms are able to estimate the values of the decision variables while running simultaneously with other control schemes. The optimization control problems work by minimizing the cost function based on vehicle dynamical model, which can be controlled by using certain constraints. For example, Tjonnas *et al*. achieved the yaw motion stability by using a nonlinear vehicle model [17]. The design worked with two modules with the objective of motion control and control allocation of actuators. The complex online nonlinear optimization problems were also used, but these problems increased the computational effort of the controller and were not appropriate for the functionality in the real scenario. To avert the problem of solving the complex nonlinear optimization, the constrained linear control allocation method was adopted instead. This method was based on linearized model and can reduce the computational complexity to the level of the quadratic programming.

Controllers designed with linear models have their own shortcomings while working in the critical conditions, such as when the vehicle dynamics alter too much in between two iterations, which can happen usually due to the fast changing tire dynamics and nonlinearities during difficult maneuvers. Linearizing the model became an option in the case but it reduces the efficiency of the controller. In some research approaches, in order to tackle the problem of reduced efficiency of the controller with the linearized model, the nonlinear model is divided into smooth piecewise linear models. To improve vehicle maneuverability and to reduce the single vehicle accidents the hybrid MPC design for coordinated control of AFS and ESP was used [19]. The prime approach was to approximate the tire-force characteristics by the piecewise affine (PWA) functions and dynamics were obtained as an affine hybrid dynamical system. Usage of nonlinear MPC was replaced by a linear time varying formulation of the MPC to avoid the computational burden. The main objective of this drive-by-wire research remains the tracking of yaw rate, also by using a switched MPC strategy [20] where the (linear and saturated) tire conditions do not change during the prediction horizon. In [21], active front steering was designed for a nonlinear model approximated by PWA model with a control strategy involving the design of two control loops. The first loop was state feedback using

a pole-placement technique designed to improve the vehicle dynamics. The second control loop, on the other hand, used a PI control that ensured the yaw rate tracking on the basis of tracking error despite constant disturbances and parameter uncertainties. In [22, 23], the partial and full automation of driving tasks were attained to increase the driver safety and to reduce the accidents by using PWA system to model the non-linearities. Also a state feedback PWA design was used on an unmanned ground vehicle (UGV) to coordinate the steering and distribution of torque input in order to minimize the vehicle skidding on difficult demanding maneuvers [24].

Using the PWA models became the pragmatic way to control the nonlinear system by designing a linear control based on linearization of the nonlinear model at different operating points. The design requirement limits the relevance of a linearization based design and stimulate the usage of PWA approximations of nonlinear models in making a control design and to expand the operating range. These PWA systems are defined as the set of linear time invariant (LTI) sub-system such that, each subsystem is a valid model of nonlinear system within the vicinity of operating points which covers the operating range of interest. The transitions in between these subsystems were modeled as "switches".

In past research, not much effort was placed in order to develop the adaptive control strategies for these type of systems. Further research although presented the adaptive control scheme for bi-modal piecewise linear systems, but its applicability was limited due to the presence of assumption in which these models were considered to be available in controllable canonical form [25, 26].

1-2 Research objectives and contribution

From the brief overview of the state-of-the-art, we can observe that the most of the research in the field to attain the vehicle yaw stability using the integrated chassis control is based on the linear vehicle model without considering the disturbances acting on these systems. The resulting control techniques work only in the linear region and are unable to handle the uncertainties in the vehicle parameters. Consequently, the adaptive control of the switched PWA vehicle systems remains comprehensively an open problem which motivates the research in this dissertation. The thesis objectives that are aimed to tackle throughout this MSc thesis are presented as below:

- **Piecewise-affine (PWA) model:** Address the vehicle yaw stability problem by adopting a piecewise-affine vehicle model in order to consider the nonlinear region of the vehicle and to expand the operating range of the controller design.
- **Hybrid adaptive approach:** Achieve asymptotic reference tracking and disturbance rejection in nonlinear vehicle models by enlarging the class of the adaptive control in the hybrid setting arising from the PWA model. Derive the stability properties of the proposed ICC algorithm.
- **Integrated Chassis Control:** Achieve system stability by integrating two active safety systems (AFS and ESP).
- **Performance during system failure:** The performance of the vehicle during a particular system (AFS or ESP) failure.
- **Validation:** Validate the control strategy by simulating the controller on a PWA and nonlinear vehicle model.

These objectives explain the need to develop the Integrated Chassis Control with the new functionalities. The hybrid adaptive approach guarantees the vehicle yaw stability in the presence of uncertainties and disturbances from the driver and its adaptation to the changing environment.

1-3 Thesis outline

The rest of the thesis is organized as follows:

Chapter 2: This chapter provides the basis of the vehicle dynamics and the methodology used in addressing the PWA vehicle model. Detailed analysis of the model and the preliminary open loop validation tests on the vehicle model are also done in this chapter.

Chapter 3: This chapter introduces a new hybrid adaptive control policy which is employed on an uncertain switched affine system. The desired tracking performance is achieved by designing the adaptive laws by using the Lyapunov function.

Chapter 4: This chapter demonstrates the effectiveness of the proposed methodology described in Chapter 3, through simulations in the presence of uncertainties and disturbances on the system.

Chapter 5: This chapter summarizes and concludes this MSc thesis with some suggestions for the future work.

Chapter 2

Vehicle Modeling

A crucial aspect in analyzing a control design is the selection of a suitable vehicle model. There exist several vehicle models, some of which have many degree of freedom and hence, can capture the dynamics of the vehicle completely but at the expense of extensive complexity and loss of physical instinct. On the other hand, simplistic models might fail to capture the complete dynamics of the vehicle. In the following methodology, a trade-off is taken between capturing relevant vehicle non-linearities, while keeping the resulting model amenable for control design.

This chapter discusses the methodology of modeling the dynamics of the vehicle to study the vehicle yaw stability based on integrated yaw moment and active front steering. In the first Section 2-1 a nonlinear vehicle model is presented assuming that the nonlinear tire forces are acting on the vehicle. In Section 2-2, the reference generator is designed to describe the set points to be tracked. In Section 2-3 a brief analysis is carried out on a nonlinear vehicle model. Section 2-4 addresses the PWA approximated model obtained from the nonlinear model. Finally, in order to validate the model an open-loop steering test is carried out in Section 2-5.

2-1 Vehicle model

A comprehensive variety of vehicle models exists in the literature which differs from one another based on the level of abstraction concerning the real systems depending upon the tires, wheel spin, aerodynamics, sprung and unsprung mass, powertrain, suspension and drive line. The bicycle model, also known as single track model, can describe the lateral dynamics of the vehicle with 2-DOF, while more advanced vehicle models may use more than 30-DOF. The choice of competent vehicle model is related to the intention of the user and on the assumptions linked to the model.

The most widely used vehicle model which can easily capture the most essential lateral steering dynamics and the yaw dynamics of the vehicle is bicycle model. This vehicle model is approximated as PWA system used for the controller design as the driver assisting system.

Further in the thesis, the nonlinear vehicle model with Pacejka tire formula is used in the simulations to validate the controller performance. The detailed description of the bicycle model is provided in the following section.

2-1-1 Chassis modeling: Bicycle vehicle model

This vehicle model describes relatively simple planer vehicle motion. The model was named as bicycle model from the fact that it used single tire 'lumped' together at subsequent axle with the cornering stiffness and force capabilities twice as that of the individual tire at the axle. This vehicle model possesses 2-DOF including lateral and yaw motion of the vehicle. For this model, there exist certain assumptions which are required to idealize the motion of the vehicle [27].

These assumptions were as follows:

1. Vehicle was subjected to move on a flat surface.
2. Left and right wheels of the vehicle at the subsequent axles were lumped into the single wheel at the centerline of the vehicle.
3. The longitudinal velocity was assumed to be constant at all times and hence, the longitudinal acceleration was always zero.
4. It is assumed that no braking was applied on the wheels individually.
5. The center of gravity was assumed to be stagnated during the braking and the acceleration (i.e. the longitudinal and lateral load transfers were neglected).
6. The vehicle structure was assumed to be rigid, including the suspension system.
7. It was assumed that the front wheels have the same steering angle.
8. The desired side-slip angle was assumed to be zero in steady-state condition.

Figure 2-1 illustrates the variables and the parameters used in this model in detail.

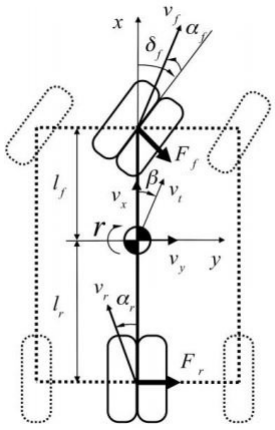

Figure 2-1: Bicycle vehicle model [1]

It was also considered that the reference frame origin was set in the vehicle center of mass, where the x-axis was along the longitudinal direction of the vehicle, the y-axis was transversal to the direction of the vehicle and the z-axis points upwards. It was also assumed that the angle was increasing in the clockwise direction.

The lateral dynamics of the vehicle can be derived by using the equation of motion. This can be done by force balance in y-direction and moment balance in z-direction.[8, 28]

$$\begin{aligned} mv_x(\dot{\beta}+r) &= 2F_f cos(\delta_f) + 2F_r \\ I_z\dot{r} &= 2l_f F_f cos(\delta_f) - 2l_r F_r + \Delta M \end{aligned} \tag{2-1}$$

where $\dot{\beta}$ was rate of change of side slip angle, $\dot{r}$ was yaw acceleration of vehicle, β was side slip angle of the vehicle and r was the yaw rate, F_f and F_r were lateral forces acting on front and rear lumped tires, δ_f was steering angle of front tire, m was the mass of the vehicle, I_z was yaw inertia (i.e. the moment of inertia about vertical axis) and ΔM was corrective yaw moment which was the result of differential braking from ESP. The constants l_f and l_r were the distance from the center of gravity (COG) of the vehicle to the front and rear axle respectively. The states of the vehicle were defined based on the frame fixed to the body of the vehicle, thus we can define a_y (lateral acceleration) relative to inertial reference frame.

$$a_y = \dot{v_y} + v_x r \tag{2-2}$$

The model equations describing the lateral motion can be written by using the lateral acceleration of the vehicle. But in this case in-spite, of using the lateral acceleration expression, the equation of motion were characterized in terms of side slip angle (β) which can best describe the conditions of the lateral slipping. β was described as the angle between the velocity vector at the center of COG and the longitudinal axis of the vehicle. This can be calculated in terms of v_y and v_x as:

$$\beta = arctan(\frac{v_y}{v_x}) \approx \frac{v_y}{v_x} \tag{2-3}$$

with the above approximation $\dot{\beta}$ can be approximated to $\dot{v_y}/v_x$.

2-1-2 Tire modeling

During vehicle modeling the forces acting on the vehicle due to aerodynamic drag was neglected. The sole reason of the forces accounted on the vehicle chassis was due to four contact patches resulting from the interaction between tire and road. Therefore, an adequate tire model becomes a necessity for the vehicle modeling and to investigate its dynamic behavior.

Tire forces

The forces and moments acting on each tire affect the dynamics of the vehicle. These are illustrated in Figure 2-2.

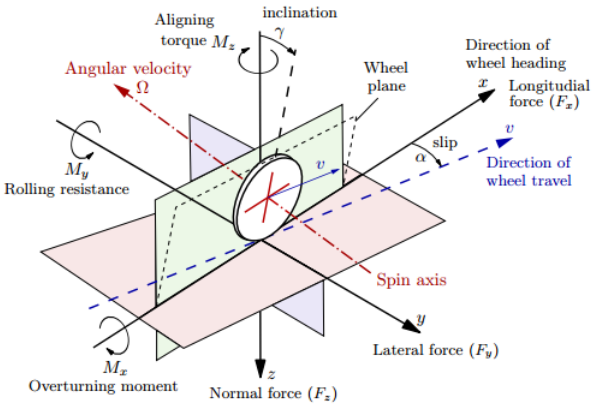

Figure 2-2: Forces and moments from the road acting on tire [2]

These forces and moments were generated by the deformations in the rubber compounds of the tire during the cornering maneuvers. A vehicle tire can sustain some amount of force before it starts losing the traction and starts to slip. Slip angle is the quantity which tells about the skidding (sliding/slipping) of the tire. Bigger the slip angle is, more the tire starts to slide. Since, we are considering the lateral dynamics we are only associated with the lateral forces (F_y) and the aligning torque (M_z) [8]. These lateral forces depends upon the side slip angle of the tire which is defined as:

Definition 2-1.1. ***Tire side slip angle*** *The side slip angle of the tire can be defined as the difference between the steering angle of the tire and the orientation of tire's longitudinal velocity. This is described by α in Figure 2-2.*

The phenomenon takes place when the tire is in cornering making the contact patch to resist the force of friction between the tire rubber and the road surface. This leads to the distortion of the tire treads due to its elastic nature. This, in turn, resists the turning action and make the tire to point in a different way than the actual desired path.

The velocity vector for every wheel can be obtained by the ratio of lateral velocity to the longitudinal velocity. The side slip angle for the front and rear tires can hence be given by the following equations:

$$\begin{aligned} \alpha_f &= \delta_f - \arctan(\beta + \frac{l_f r}{v_x}) \\ \alpha_r &= -\arctan(\beta - \frac{l_r r}{v_x}) \end{aligned} \tag{2-4}$$

Usually, the side slip angles are assumed to be small at higher speed and hence the above equations can be written as follows:

$$\begin{aligned} \alpha_f &= \delta_f - (\beta + \frac{l_f r}{v_x}) \\ \alpha_r &= -(\beta - \frac{l_r r}{v_x}) \end{aligned} \tag{2-5}$$

After defining the lateral wheel side slip angle, the next section investigates on how these terms are related to the tire forces.

2-1-3 Pacejka's tire model

The discrepancies in the handling properties of the vehicle can be described evidently by the forces acting on the tires. So, the selection of the realistic model for this purpose was quite crucial. The model which can correctly express the non-linearities and the uncertainties in the tire characteristics was preferred. The *Pacejka's* tire model also known as *Magic Formula* contributes a technique to calculate the longitudinal and lateral tire forces and the aligning moment for the vehicle. The validity of this model was available for quite a large domain of slip ratio and slip angles [3].

The above mentioned tire model can be described in general by the equation as follows:

$$\begin{aligned} Y(x) &= y(x) + S_v \\ x &= X + S_h \end{aligned} \tag{2-6}$$

These nonlinear characteristic can be observed in Figure 2-3. The output Y can either be the lateral force or the longitudinal force whereas, x was the function of tire slip angle (or slip ratio). Categorically this curve can be divided into three distinct zones. The first region contain moderate values of the side slip angle (or slip ratio) corresponding to the standard driving conditions. In this region, the lateral dynamics were not so demanding and the relationship between side slip angle and lateral forces can be considered linear. The side slip angle increased further in the second region and tire reach its sliding behavior. The tire forces in this region were not linear with the side slip angle and slip starts to occur. So, we need certain control strategy that can help to reduce the side slip angle when tire forces were nonlinear. In the third region, the tire forces reaches its extreme value and then saturates.

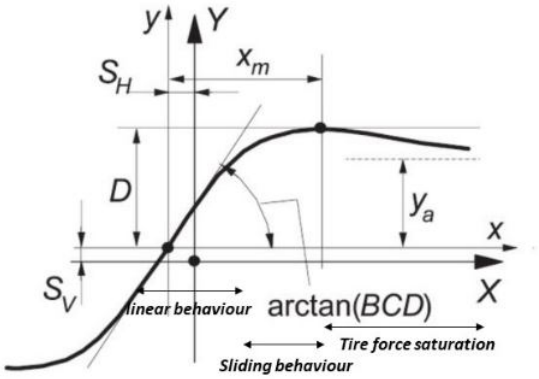

Figure 2-3: Magic formula [3]

The formula used numerous coefficients to determine the trends in forces and moments. These coefficients were explained in Table 2-1. The coefficients S_v and S_h are used to avoid symmetrical asymptote about the origin. This can be understood as the offset from the origin caused by the

Table 2-1: Magic formula coefficients

Coefficient	Coefficient Name
B	Stiffness Factor
C	Shape Factor
D	Peak Factor
E	Curvature Factor
S_h	Horizontal Shift
S_v	Vertical Shift

presence of the camber angle (described as angle between the vertical axis of the wheels used for steering and the vertical axis of the vehicle when viewed from the front or rear).

Considering the disjoint case, with the lateral or longitudinal force with pure slip. The generation of tire forces can be expressed by the following equation:

$$\begin{aligned} F_f &= D_f \sin(C_f \arctan(B_f\alpha_f - E_f(B_f\alpha_f - \arctan(B_f\alpha_f)))) \\ F_r &= D_r \sin(C_r \arctan(B_r\alpha_r - E_r(B_r\alpha_r - \arctan(B_r\alpha_r)))) \end{aligned} \tag{2-7}$$

These two equations represent the generation of lateral forces in front F_f and rear F_r tire respectively and α_f and α_r are side slip angle for front and rear tires. S_v which can be understood as the offset from the origin is zero due to the assumption of camber angle to be zero.

2-2 Desired vehicle response

In this section, the response desired by vehicle was characterized as the yaw stability control objectives. The model used in this dissertation requires the desired response for its characteristic states. Yaw rate (r) and side slip angle (β) are the significant variables for the vehicle yaw stability control. These values served as the reference state values when the given control problem was presented in the form a tracking problem. From [3] the control objectives of the yaw stability control can be classified as yaw rate control, side slip angle control and combination of both as illustrated in Figure 2-4.

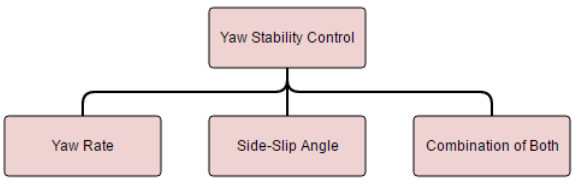

Figure 2-4: Yaw stability control objectives

One such objective is controlling the yaw rate (r). Keeping the actual yaw rate of the vehicle close to the desired yaw rate response can enhance the handling or maneuverability of the vehicle. In

steady state condition, the desired yaw rate (r) response can be achieved by using (2-8)

$$r_d = \frac{v_x}{(l_f + l_r) + k_{us} v_x^2} \delta_f \tag{2-8}$$

where k_{us} is the stability factor or understeer gradient depending upon the vehicle parameters. The increase in k_{us} results in the lower desired yaw rate demanding a more understeer response of the vehicle. It is defined in (2-9)

$$k_{us} = \frac{m(l_r c_r - l_f c_f)}{(l_f + l_r) c_f c_r} \tag{2-9}$$

Remark 2-2.1. *The stability analysis of the vehicle system can be done by observing the sign of the magnitude of the constant k_{us}. If $k_{us} > 0$, the vehicle system is in understeer behavior which is considered to be the stable system. In this scenario ($\alpha_f > \alpha_r$). If $k_{us} = 0$, the vehicle remains stable and the behavior is called as neutral steer. Here, ($\alpha_f = \alpha_r$). In the case when $k_u s < 0$, the vehicle is in oversteer behavior and is unstable if the vehicle is coasting above a particular critical velocity defined by $\sqrt{\frac{-(l_f+l_r)}{k_{us}}}$. The ($\alpha_f < \alpha_r$) in this case.*

These vehicle behavior was shown in Figure 2-5

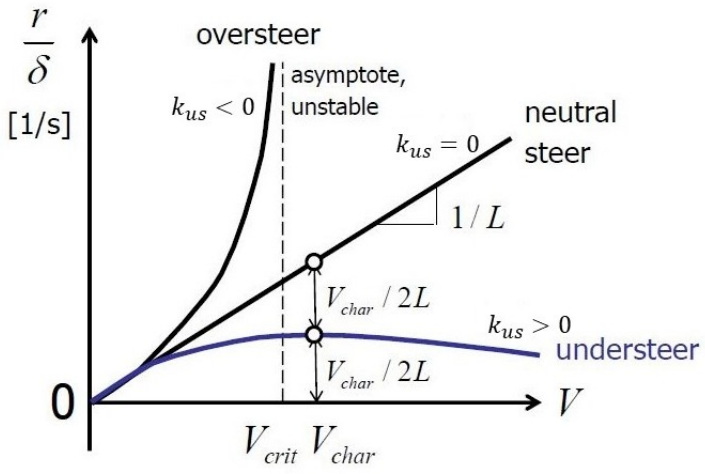

Figure 2-5: Lateral vehicle dynamics behavior [4]

During neutral behavior, the vehicle follows the desired path and driver can keep a constant steering angle, independent of the vehicle velocity to make a safe maneuver. During understeer, the vehicle slides outwards of the corner and in order to maintain the desired trajectory, the steering angle has to be increased. On the other hand, during oversteering, the vehicle turns too slow and the front axle is not able to generate enough later force leading the vehicle to slide inwards of the corner. So, in order to maintain the desired trajectory the steering angle has to be reduced or in extreme conditions, the counter-steering is applied to make a safe turn.

The other control objective was to control the vehicle side slip angle (β), which was the angle of deviation in between vehicle longitudinal axis and its direction of motion. By keeping the side slip angle close to the steady state condition, assures the lateral stability of the vehicle. For steady state condition, the desired side slip angle was considered zero ($\beta_d = 0$). So, in order to ensure the proper vehicle handling and stability performance, it was crucial to control both the system responses.

The friction coefficient acting between the tires and the road surface limits the maximum yaw rate. To allow the vehicle to make a safe maneuver at the given speed the vehicle require higher yaw rate but at the expense of the large side slip angle, which can make the system response unstable. Hence, the yaw rate defined in (2-8) has to be accustomed depending upon the conditions of the road. The maximum desired yaw rate can be described by (2-10) [8].

$$r_{d_{max}} = 0.85 * \frac{\mu g}{v_x} \tag{2-10}$$

2-3 Vehicle model analysis

A nonlinear vehicle model usually has a limited stability region, this region includes a stable equilibrium point (trivial solution) and two saddle points (non-trivial solution). The system in the region with the positive slope has only one equilibrium solution, whereas the other two symmetrical unstable equillibria will appear when the system works in decaying nonlinear region. This region of stability varies with various factors such as steering angle, longitudinal velocity, and friction in between road and tire. The effects of change in steering angle keeping the velocity and coefficient of friction as constants, on stability region of the vehicle was analyzed by the phase portrait diagrams. These diagrams can completely describe the dynamics of the system as well as the stability of the equilibrium point. The phase portraits were usually generated by simulating the model at various initial conditions and plotting the resulting trajectories in the state space. The attractive domain for the stable trivial solution was spanned by the area of stable manifolds. The vehicle working outside this manifold will experience instability (representing vehicle spin). The phase portraits were shown below with simulations carried out on the nonlinear vehicle model (2-1) with nonlinear tire forces given by (2-7). The model parameters used for this case are defined in Appendix A.

Figure 2-6 represent the state trajectories for a vehicle traveling on the road, with front steering control. The trajectories were attracted towards the globally stable equilibrium point with steering angle= 0 [rad] (i.e. the straight line vehicle traveling). Other scenarios were also discussed, where the steering angle of 0.03 [rad] was commanded by the driver (i.e. left steering corresponding to left cornering). The point of equilibrium gets shifted from the origin and the state trajectories are attracted towards this new equilibrium point.

It can be stated in this sense, that if the steering angle commanded by the driver changes from the center position, the movement of the vehicle changes from the straight line traveling to the cornering. If this movement of the steering wheel was large, then the stable equilibrium point will disappear which can be seen in Figure 2-7. In this scenario, the vehicle enter the divergent state and falls into a spin. This makes it impossible to achieve the required yaw velocity without any

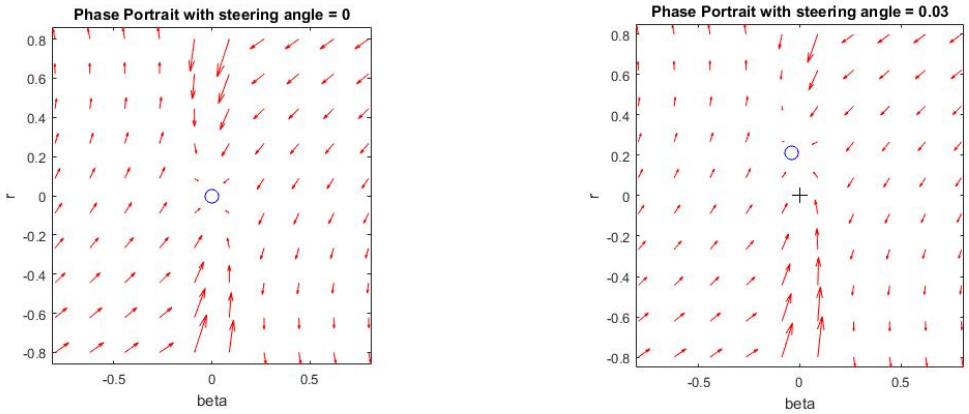

(a) Steering angle = 0 [rad] **(b)** Steering angle = 0.03 [rad]

Figure 2-6: Phase portrait analysis of vehicle with change in steering angle

control. So, in order to achieve large value of steady yaw rate to prevent vehicle spin, we require vehicle dynamic control [29].

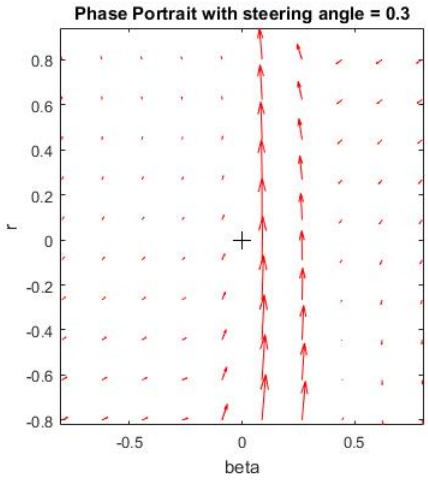

Figure 2-7: Phase portrait for steering angle = 0.3 [rad]

2-4 Piecewise affine vehicle model

The nonlinear 2-DOF vehicle model in (2-1) was approximated as a PWA system. This can be done by partitioning of the nonlinear lateral tire forces into the polyhedral sets such that for each region, an affine system was used to describe the linearized dynamics. This approach was used to approximate the non-linearities to arbitrarily precision [19].

The Pacejka's tire model was approximated as PWA functions: The lateral tire force acting on the front tire was approximated by the following function $F_f(\alpha_f)$

$$F_f(\alpha_f) = \begin{cases} d_f\alpha_f - e_f & if, -\hat{\alpha_f} < \alpha_f \\ c_f\alpha_f & if, -\hat{\alpha_f} < \alpha_f < \hat{\alpha_f} \\ d_f\alpha_f + e_f & if, \alpha_f > \hat{\alpha_f} \end{cases}$$

For the consideration of this model it was assumed that the vehicle mostly has the under-steering behavior and therefore, the nonlinear characteristics of the front tire were taken into account. The rear tire forces $F_r(\alpha_r)$ were assumed to be linear.

$$F_r(\alpha_r) = (c_r\alpha_r)$$

where, d_f,e_f depends upon the front tire forces corresponding to the partitioning of tire force domain, based on slip angle (α_f). A similar kind of approach can be employed to the vehicles with over-steering behavior. This research was intended to consider three regions in the PWA model for the purpose of synthesizing control, so as to reduce the number of constraints [30]. The regions were bounded by symmetrical threshold values of $\alpha_f = \pm\hat{\alpha_f}$, shown in Figure 2-8. The parameters used to describe the PWA model were expressed in Appendix B

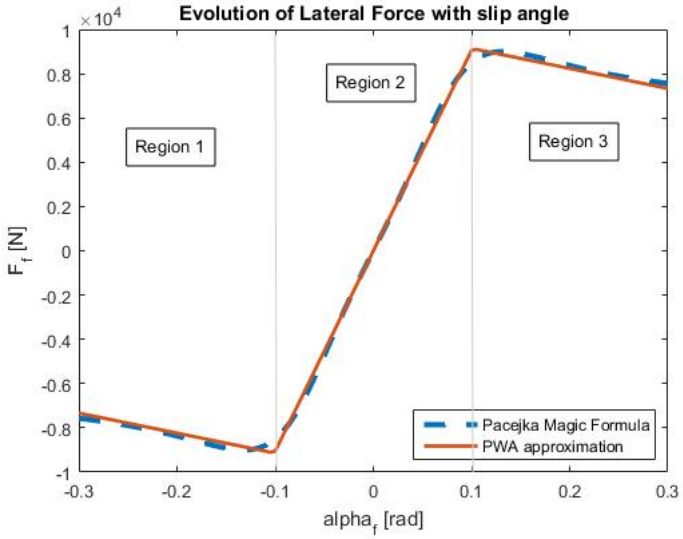

Figure 2-8: Pacejka magic formula for front tire force and PWA approximation according to partitioning of tire sideslip angle domain in three operating regions.

Now, the nonlinear system represented by (2-1) was linearized around uniform rectilinear motion (i.e. v_x = constant, $\beta = 0$, $r = 0$, $\delta_f = 0$) and considering the PWA affine functions used to approximate non-linear tire forces. The vehicle dynamics can be represented as PWA system:

$$\dot{x} = A_i x + B_i u + f_i \tag{2-11}$$

$$x = \begin{bmatrix} \beta & r \end{bmatrix} \qquad \text{and} \qquad u = \begin{bmatrix} \delta_f & \Delta M \end{bmatrix}$$

with the dynamics as:

$$A_i = \begin{pmatrix} -\frac{2d_{fi}+2d_{ri}}{mv} & -1-2\frac{d_{fi}l_f-2d_{ri}l_r}{mv^2} \\ -2\frac{d_{fi}l_f-2d_{ri}l_r}{I_z} & -2\frac{d_{fi}l_f^2+2d_{ri}l_r^2}{I_z v} \end{pmatrix} \quad B_i = \begin{pmatrix} 2\frac{d_{fi}}{mv_x} & 0 \\ 2\frac{d_{fi}l_{fi}}{I_z} & \frac{1}{I_z} \end{pmatrix} \quad f_i = \begin{pmatrix} \mp 2\frac{e_{fi}+e_{ri}}{mv_x} \\ \mp 2\frac{e_{fi}l_{fi}-e_r l_r}{I_z} \end{pmatrix}$$

where, the control input was front steering angle (δ_f) and the differential yaw moment (ΔM). β and r were the state variables which were side slip angle and yaw rate respectively. Most often the PWA system partitions were expressed in terms of state-space variables. The PWA system, (2-11) can be written in terms of α_f and α_r. The switching in between these PWA sub-systems depend upon the front tire slip angle as described through the approximation of tire force function ($F_f(\alpha_f)$). This guard condition can be written in the form of state variables and control input. The switching or the guard conditions were explained through the hybrid automaton in Figure 2-9. Here the β_0 and r_0 are the initial states.

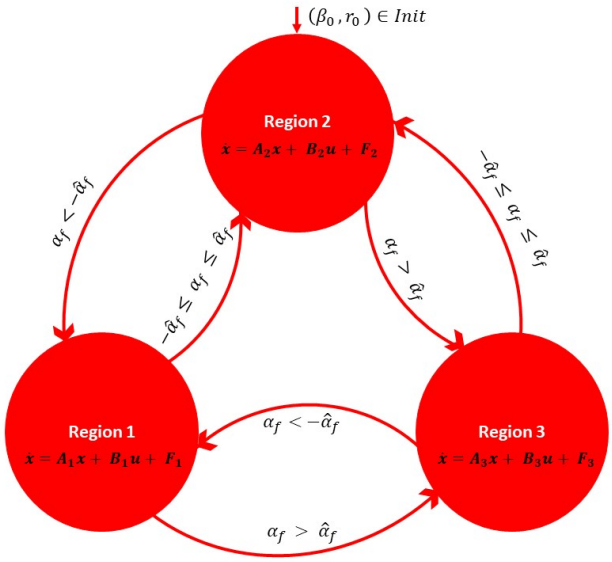

Figure 2-9: Hybrid automaton: Switching or transitions in between PWA subsystems

Remark 2-4.1. ***Linear vehicle model*** *Considering the PWA system* (2-11) *linear vehicle model can be obtained by considering linearization valid for complete domain of tire forces. This make vehicle to work in single operating region which uses linear tire force approximation obtained by using* $e_{fi} = 0$, $e_{ri} = 0$, $d_{fi} = c_f$ *and* $d_{ri} = c_r$. c_f *and* c_r *are cornering coefficients and can be obtained from the parameters of the* $Pacejka's$ *formula.*

$$c_f = B_f C_f D_f \qquad and \qquad c_r = B_r C_r D_r$$

For every corresponding vehicle state, the front and rear tire slips can be computed using equation (2-5). This in return helps in computing the lateral tire forces, which can be linked with the system to know the state information.

It was crucial to evaluate the dynamics of the vehicle before employing different control techniques on it. The analysis of vehicle system dynamics was largely based on the stability issues. A natural

starting point that investigates this phenomenon was the analysis of the steady-state cornering situation which corresponds to the equilibrium of the system.

Definition 2-4.1. *[31] **Equilibria** of the system is the state location corresponding to certain input value such that the state derivatives of the system become zero.*

$$\dot{x} = f(x_{eq}, u_{eq}) = 0 \tag{2-12}$$

The analysis of these equilibria were required to have a clear idea of the control design. The equilibrium points for this system were the pair of (β_{eq},r_{eq}). The stability of this system was decided by the following Jacobian Matrix (state matrix from linear 2-DOF bicycle model):

$$J(\beta_{eq}, r_{eq}) = \begin{bmatrix} \frac{-2c_f-2c_r}{mv_x} & \frac{-2c_f l_f+2c_r l_r}{mv_x^2} - 1 \\ \frac{-2c_f l_f+2c_r l_r}{I_z} & \frac{-2c_f l_f^2-2c_r l_r^2}{I_z v_x} \end{bmatrix}$$

where c_f and c_r were cornering stiffness of the tire, which were generally the gains obtained by local linearization between slip angle and tire forces at equilibrium for the front and rear tires respectively. In order to satisfy the stable equilibrium, certain conditions have to be satisfied. These conditions were as follows:

- trace(J) < 0, i.e $2I_z(c_f + c_r) + 2\mathrm{m}(c_f\ l_f^2 + c_r\ l_r^2) > 0$
- det(J) > 0, i.e $c_f\ c_r\ (l_f + l_r) > \mathrm{m} v_x^2 (c_f\ l_f$ - $c_r\ l_r)$

Remark 2-4.2. *[31] General cases for the stability of the system.*

- *When the slope corresponding to the lateral force and slip angle for the front and rear tire are positive (i.e. $c_f > 0$ and $c_r > 0$), the system stability can be described by $c_f l_f - c_r l_r \leq 0$. The (< 0) in this inequality, represents understeer behavior whereas the ($= 0$), represents neutral steer. When $c_f l_f - c_r l_r > 0$ the system is conditionally stable, with the following condition to be followed:*

  $$v_x < \sqrt{\frac{c_f c_r l^2}{m(c_f l_f - c_r l_r)}} \tag{2-13}$$

  This case represents the over-steer condition for this system. Small steering angles will allow the vehicle to remain in linear region with understeer behavior

- *When $c_f < 0$ and $c_r > 0$, the front tire works in decaying region and $c_r > c_f$ makes $trace(J) < 0$. The system stability remain conditional with the following condition to be satisfied.*

  $$v_x > \sqrt{\frac{|c_f| c_r l^2}{m(|c_f| l_f - c_r l_r)}} \tag{2-14}$$

- *When $c_f > 0$ and $c_r < 0$, the rear tire works in decaying region. This condition makes equilibrium point a saddle point and system becomes unstable as $det(J) > 0$.*

- *When $c_f < 0$ and $c_r < 0$, both tires works in decaying region. The system tends towards instability as $trace(J) > 0$.*

In order to validate the PWA vehicle model the open-loop steering test were carried on the vehicle model. This test consists of the system open-loop response against two steering inputs from the driver which are ramp and sine with dwell. This test was conducted as follows:

2-5 Open-loop steering test

2-5-1 Ramp steering

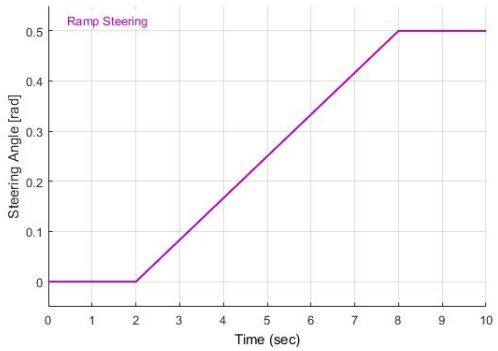

Figure 2-10: Ramp steering angle

In the simulation environment, the vehicle was allowed to move at the constant longitudinal velocity of 20 m/s with the front steering angle increasing from 0 to 0.5 rad in 6s. The steering angle was kept constant to 0.5 rad after 6s. Figure 2-10 represent the given steering angle.

The vehicle simulations were obtained with no controller in the loop. The results obtained were as follows:

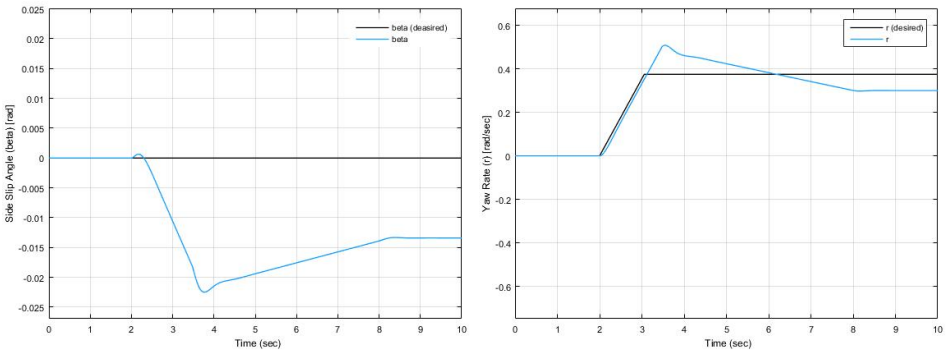

(a) Side slip angle with no control **(b)** Yaw rate with no control

Figure 2-11: System response with ramp steering at constant velocity 20 m/s

It was observed that the ramp steering was able to excite the nonlinear tire dynamics and with no control in the loop the system becomes unstable and the side slip angle was no longer bounded anymore. The reference tracking does not occur for both the side slip angle and yaw rate of the vehicle. The performance loss can be observed by the overshoot in yaw rate. With no control, an overshoot of 31.6% was observed and the proper control technique will be required to bound the yaw rate to the desired yaw rate. The performance loss due to the increase in steering angle can be foreseen as the front tires enter the nonlinear region considerably further from the rear tires. This situation was the result of the application of the higher steering angle by an average driver in difficult maneuvering conditions.

2-5-2 Sine with Dwell (SWD)

To check the performance of the ESP on the vehicle, sine with dwell (SWD) test was used. The performance requirements for the control of the vehicle in this test were specified in the USA regulation FMVSS 126 [32]. All international regulations like Global Technical Regulation No. 08 electronic stability control system, require the ESP performance to be demonstrated by using the SWD maneuvering test.

This test maneuver allows the vehicle to coast at constant longitudinal velocity with the driver steering wheel input with a sine wave having a frequency of 0.7 Hz and a delay of 500 ms in between the first and second peak amplitude as shown in Figure 2-12. According to the FMVSS No. 126 there exist two criteria to check the lateral stability of the vehicle.

$Criterion$ 1 states that the instant yaw rate of the vehicle after 1 sec of the completion of the steering should be 35% or less than the peak rate produced by the steering reversal.

$$Criterion_1 = \frac{r_{t_0+1}}{r_{peak}} * 100\% \leq 35\% \tag{2-15}$$

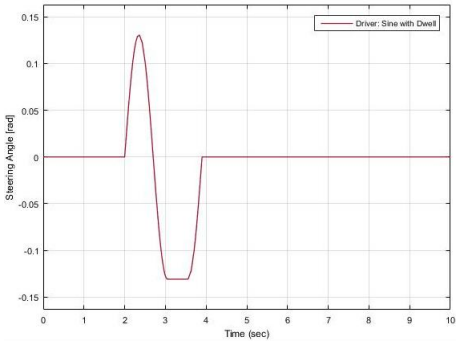

Figure 2-12: Sine with Dwell steering angle

On the other hand, $criterion$ 2 states that the instant yaw rate must be 20% or less than the peak yaw rate produced by the steering reversal.

$$Criterion_2 = \frac{r_{t_0+1.75}}{r_{peak}} * 100\% \leq 20\% \tag{2-16}$$

The vehicle simulations for SWD maneuver were obtained with no controller in the loop. The results obtained were as follows:

It can be observed from the vehicle response that, the vehicle side-slip angle and yaw rate became quite large, as can be seen, the overshoot of about 52.64% can be observed in the yaw rate response. This makes the vehicle to slide outwards of the corner. To follow the reference and to allow the vehicle to work in the safe region the driver has to increase the steering angle to maintain the desired trajectory. But, this type of situation can be overcome by the expert drivers. For the regular drivers, the controller is required to bound the side slip angle and to generate the required yaw rate (lateral acceleration) to stabilize the system.

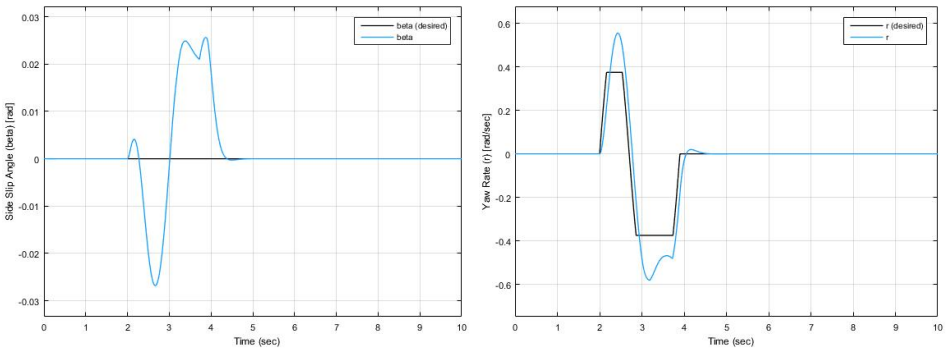

(a) Side slip angle with no control **(b)** Yaw rate with no control

Figure 2-13: System response with Sine with Dwell steering at constant velocity 20 m/s

Table 2-2: Open-loop system performance

No Control	Ramp Steering	Sine with Dwell
overshoot in $'\beta'$	2.3 %	2.9 %
overshoot in $'r'$	31.6 %	52.64 %

To penalize the large overshoot in both β and r response of the system as described in Table 2-2 a superior ICC control strategy is required.

2-6 Summary

In this chapter, a PWA vehicle model was formulated from the nonlinear model by approximating the nonlinear tire forces as PWA functions. The desired reference generator was also obtained and a brief system analysis was done by performing the open loop test. The next chapter gives a detailed idea of the design of the hybrid adaptive control policy used to achieve the desired stability and tracking properties.

Chapter 3

Hybrid Adaptive Control Policy

In this chapter, state tracking control problem was devised for multiple-input PWA systems using the state feedback control. The organization of the chapter is as follows: Section 3-1 formulates the problem statement. Section 3-2 establish the adaptive state feedback control design with subsections presenting the stability and tracking results.

3-1 Problem statement

This dissertation consider the multi-input PWA system obtained by linearizing and approximating a nonlinear system at multiple operating points, which is described as follows:

$$\dot{x} = A(t)x(t) + B(t)u(t) + f(t) \tag{3-1}$$

where,

$$A(t) = \sum_{i=1}^{l} A_i \chi_i(t) \qquad B(t) = \sum_{i=1}^{l} B_i \chi_i(t) \qquad f(t) = \sum_{i=1}^{l} f_i \chi_i(t) \tag{3-2}$$

The parameters $A(t)$, $B(t)$, $f(t)$ varies in PWA pattern, i.e. the value of set ($A(t)$, $B(t)$, $f(t)$) takes on different values at different time periods which were specified by the parameter matrix set (A_i, B_i, f_i), representing the dynamics of the controlled plant at distinct operating points. These dynamics were the region of interest for all possible system state and control vector (x, u). These regions were represented as $\Omega_i \subset \mathbb{R}^{n+m}$, where n and m were dimensions of state vector (x) and control input (u) respectively and set of these regions are represented by $i \in I \triangleq (1, 2, ..., l)$. To describe the parameter discontinuities and for integrity of notation, the indicator function was introduced [33].

$$\chi(t) = \begin{cases} 1 & if, (x(t), u(t)) \in \Omega_i \\ 0 & otherwise \end{cases} \tag{3-3}$$

This function was used due to the assumption that the common boundary of the two regions will belong to the either of the two regions. This function also contained the information of time duration of parameter matrix set ($A(t)$, $B(t)$, $f(t)$) and the time instants at which the switching occurs from one region to another. Since, the information about $(x(t), u(t)) \in \Omega_i$ was available, the indicator function defined in (3-3) was known.

The control objective of this dissertation is to establish a state feedback control law for the plant (3-1) *so that all the signals in the closed-loop system are bounded and state vector* $x(t)$ *tracks the reference trajectory* $(x_m(t))$ *(generated from reference model) asymptotically.*

3-2 Adaptive state feedback control

In most of the control system problems, the state feedback was used, due to its transparent structure and robust functions. Before developing an adaptive control, it was crucial to determine the associated non-adaptive control problem. When the parameters of the controlled plant were available and given control objectives have to be followed, it became important to design a nominal controller identical to the set of the matching conditions. To ensure the closed loop stability and desired tracking in the case when the plant parameters were unknown, the adaptive scheme was required to update the controller parameters.

3-2-1 Time-varying reference model system

This approach assume that the states of the controlled system were available for measurement. In order to attain the desired trajectory for these states a reference model was chosen to be LTI. Nonetheless, this LTI reference system impose stringent structural requirements on constituent piecewise affine subsystems. This require matching the same behavior of each subsystem with a common LTI reference model through nominal controller parameters. This was not feasible in most of the practical applications and hence, to describe a realistic scenario it was required to specify LTI reference model for each subsystem established on the knowledge of the desired response at different operating points. Desired behavior of each subsystem and the transitions in between these subsystems were specified locally as the reference trajectory $x_m(t)$.

The reference model was specified individually for PWA system. For each subsystem, the state trajectory $x_m(t)$ was desirable for the perturbed state $x(t)$ to follow. To form a global reference trajectory for $x(t)$ to track the $x_m(t)$, the resulting set of the LTI (linear time invariant) reference model was needed, which was described as:

$$\dot{x}_{mi}(t) = A_{mi}x_{mi}(t) + B_{mi}r(t) + f_{mi} \tag{3-4}$$

where $r(t) \in \mathbb{R}^n$ was a bounded continuous reference input signal, and the parameter matrices $A_{mi} \in \mathbb{R}^{n*n}$, $B_{mi} \in \mathbb{R}^n$, $i \in I$, were chosen with A_{mi} stable (Hurwitz). Here, $x_m(t)$ was needed to be a

continuous reference trajectory so as to be followed by continuous state vector $x(t)$. Therefore the reference state reset at the time when the switching occurs from i^{th} to j^{th} at a time instant t.

Stability of the reference model system

The stability properties of the reference model were examined without considering the offset term f_{mi} in the dynamics of the PWA system. By using the similar approach as in literature [34, 5, 35] it can be proved that the exponential stability of the homogeneous system entails the stability of the piecewise reference model (3-4). The stability of the reference model at switching time instants T_0 can be proved by the Lyapunov equation:

$$A_{mi}^T P_{mi} + P_{mi} A_{mi} = -Q_{mi} \tag{3-5}$$

such that the P_{mi}, $Q_{mi} \in \mathbb{R}^{n*n}$ were symmetric and positive definite.

Since A_{mi} was Hurwitz, there exist a_{mi},$\lambda_{mi} > 0$ such that $||e^{A_{mi}t}|| \leq a_{mi}e^{-\lambda_{mi}t}$. Define $a_m = \max_{i\in I} a_{mi}$, $\lambda_m = \min_{i\in I}\lambda_{mi}$, $\alpha = \max_{i\in I}\lambda_{\max}\,[P_{mi}]$, $\gamma = \min_{i\in I}\lambda_{\min}\,[P_{mi}]$, where $\lambda_{\min}[.]$, $\lambda_{\max}[.]$ represents the minimum and maximum eigenvalues of a matrix respectively. The exponential stability of the homogeneous system and hence, the reference model system can be ensured by the lower bound on T_0 given by the following lemma.

Lemma 3-2.1. *[36] The homogeneous system of a reference model system* (3-4)*, $\dot{z} = A_m(t)z(t)$, is exponentially stable with decay rate of $\varsigma \in (0, 1/2\alpha)$, if the minimum switching time interval is such that*

$$T_0 \geq \frac{\alpha}{1-2\varsigma\alpha}\ln(1+\mu\Delta_{A_m}), \qquad \mu = \frac{a_m^2}{\lambda_m\gamma}\max_{i\in I}||P_{mi}|| \tag{3-6}$$

and $\Delta A_m = \max_{i,j\in I}||A_{mi} - A_{mj}||$ is the largest difference between any two subsystems.

Proof. Let the subsystem of the (3-4) is denoted by $A_{m(k-1)} \in (A_{m1}, ..., A_{ml})$, $k \in \mathbb{Z}^+$. Consider switching at $t = t_k$. Because of the stability of $A_{m(k-1)}$ and $A_{m(k)}$ and without loss of generality, there exist symmetric and positive definite matrix $P_{m(k-1)}$ and $P_{m(k)} \in \mathbb{R}^{nxn}$ such that

$$\begin{aligned} A_{m(k-1)}^T P_{m(k-1)} + P_{m(k-1)} A_{m(k-1)} &= -I_n \\ A_{m(k)}^T P_{m(k)} + P_{m(k)} A_{m(k)} &= -I_n \end{aligned} \tag{3-7}$$

$I_n \in \mathbb{R}^{nxn}$ is identity matrix and $\Delta A_{m(k)} = A_{m(k)} - A_{m(k-1)}$, $\Delta P_{m(k)} = P_{m(k)} - P_{m(k-1)}$, thus

$$A_{m(k)}^T \Delta P_{m(k)} + \Delta P_{m(k)} A_{m(k)} = -S_{(k)} \tag{3-8}$$

$$S_{(k)} = \Delta A_{m(k-1)}^T P_{m(k-1)} + P_{m(k-1)} \Delta A_{m(k-1)} \tag{3-9}$$

Also, $||S_{(k)}|| \leq 2||P_{m(k-1)}||\,||\Delta\, A_{m(k)}||$. Since $A_{m(k)}$ is Hurwitz, the solution to (3-8) is

$$\Delta P_{m(k)} = \int_0^\infty e^{A_{m(k)}^T t} S_{(k)} e^{A_{m(k)} t} dt \tag{3-10}$$

and when $||e^{A_{mi}t}|| \leq a_{mi}e^{-\lambda_{mi}t}$ then (3-10) leads to

$$||\Delta P_{m(k)}|| \leq \frac{a_m^2}{\lambda_m}||P_{m(k-1)}||||\Delta A_{m(k)}|| \tag{3-11}$$

Considering a continuous piecewise Lyapunov function

$$V = z^T(t)\sum_{i=1}^{l} P_{mi}\chi_i z(t) \tag{3-12}$$

here P_{mi} satisfies (3-5). At inequality (3-11) and when $\gamma||z(t)||^2 \leq V$, then the equation is updated to

$$V(t_k) - V(t_{k-1}) = z^T(t_k)\Delta P_{m(k)} z(t_k) \leq \frac{a_m^2}{\lambda_m \gamma}||P_{m(k-1)}||||\Delta A_{m(k)}||V(t_{k-1}) \tag{3-13}$$

Now when $\mu = \frac{a_m^2}{\lambda\gamma} max_{i\in I}||P_{mi}||$, follows $V(t_k) \leq (1+\mu\Delta_{A_m})V(t_{k-1})$. In addition, with $V \leq \alpha||z(t)||^2$, the time derivative of V satisfies $\dot{V} \leq -V/\alpha$ and

$$V(t) \leq e^{\frac{-1}{\alpha}(t-t_0)}(1+\mu\Delta_{A_m})^{k-1}V(t_0)$$

leading to

$$||z(t)|| \leq \frac{\alpha}{\gamma}^{\frac{1}{2}} e^{\frac{-1}{2\alpha}(t-t_0)+\frac{k-1}{2}} \ln(1+\mu\Delta_{A_m})||z(t_0)||$$

Also, T_0 being the minimum switching time interval $t - t_0 \geq (k-1)T_0$ together with condition (3-6) gives,

$$\frac{-1}{2\alpha}(t-t_0) + \frac{k-1}{2}\ln(1+\mu\Delta_{A_m}) \leq -\varsigma(t-t_0)$$

and hence insures the exponential stability. □

Remark 3-2.1. *The condition* (3-6) *relates a lower bound on minimum switching time interval which was required for the exponential stability of the system explicitly to the largest difference* Δ_{A_m} *between the subsystems of the reference model* (3-4)*. When all constituent reference model were same and* Δ_{A_m} *reduces to zero, the exponential stability was followed for the arbitrary switching in the system. Equivalent conclusion can be drawn in the presence of the common Lyapunov matrix* P_m *such that* $A_{mi}^T P_m + P_m A_{mi} < 0$.

Consider the system with two PWA affine subsystems and let t_i, $i = 1,2,...$ be the switching time instants. Let V_a and V_b be the Lyapunov functions which were radially unbounded. In case, when a common P_m exists, the values of V_a and V_b coincide at each switching time, i.e., $V_{\sigma(t_{i-1})}(t_i) = V_{\sigma(t_i)}(t_i)$ for all i, and then V_σ was a continuous Lyapunov function for the switched system. This allow the asymptotic stability to follow. This situation was depicted in Figure 3-1(a).

In case, when no common P_m exist, V_σ was discontinuous function. Each Lyapunov function decrease when the corresponding subsystem was active, it may or may not increase when the subsystem becomes inactive. The switched system was globally asymptotically stable if the value of all Lyapunov functions was a decreasing sequence from the beginning of each interval. This situation was depicted in Figure 3-1(b).

3-2-2 Adaptive control design

This subsection explains a state feedback control structure and the adaptive laws developed for the control of piecewise affine plant (3-1). The defined technique can ensure the closed loop stability

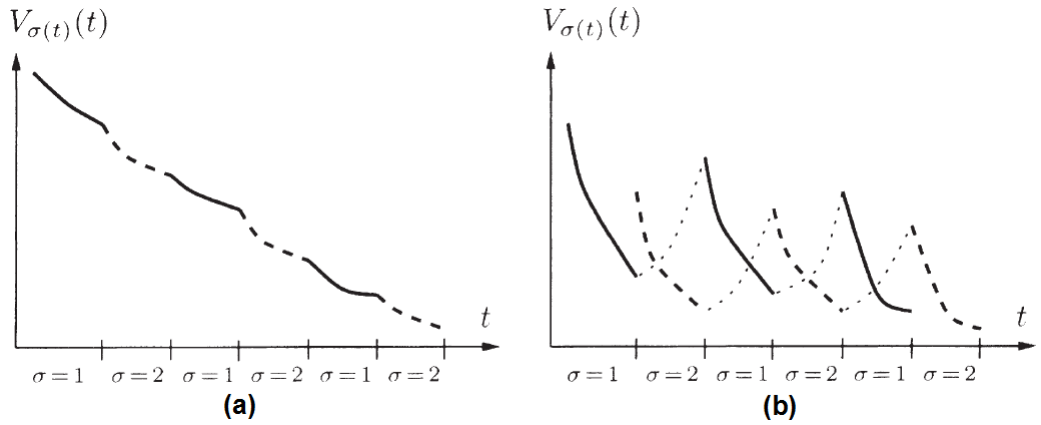

Figure 3-1: Different Lyapunov functions (solid lines corresponding to V_a, dashed lines corresponding to V_b): a). continuous common V_σ, b). discontinuous V_σ [5]

(signal boundedness) and asymptotic state tracking of a given reference state even in the presence of disturbances. In order to have a well-posed adaptive problem certain assumptions were made which were as follows:

Assumption 1. *There exist a constant matrix $K_i^* \in \mathbb{R}^{nxm}$ and a non-singular (invertible) constant matrix $L_i^* \in \mathbb{R}^{mxm}$, such that*

$$A_{mi} = A_i + B_i K_i^{*T} \qquad B_{mi} = B_i L_i^* \tag{3-14}$$

Assumption 2. *There exists known matrices $S_i \in \mathbb{R}^{mxm}$, such that G_i are symmetric and positive definite matrix*

$$G_i = L_i^* S_i \tag{3-15}$$

Assumption 3. *There exist a constant matrix $M_i^* \in \mathbb{R}^{mxm}$, such that*

$$f_{mi} = f_i + B_i M_i^* = 0 \tag{3-16}$$

Remark 3-2.2. *Assumption* 1 *was called the matching condition and was needed so as to ensure the presence of the closed loop that match* (3-1) *the reference model* (3-4) *for a well-posed adaptive problem. Assumption* 2 *conclude the classical condition to recognize the sign of the magnitude of input vector field in the multi-variable case. Assumption* 3 *was required to compensate the effect of the affine terms on the system. These assumptions till now were in their most casual conditions to ensure the boundedness of the closed loop signal in the case of adaptive multi-variable control and were selected to design our control problem [37, 38].*

Controller structure and error model

In the particular case when the plant parameters were known (as in the case of reference model), the nominal control law was followed to achieve the closed loop stability of the system.

$$u(t) = K^{*T}(t)x(t) + L^*(t)r(t) + M^*(t) \tag{3-17}$$

where,

$$K^*(t) = \sum_{i=1}^{l} K_i^* \chi_i(t) \qquad L^*(t) = \sum_{i=1}^{l} L_i^* \chi_i(t) \qquad M^*(t) = \sum_{i=1}^{l} M_i^* \chi_i(t) \tag{3-18}$$

This control law would result in the closed loop system:

$$\dot{x}(t) = A_i x(t) + B_i(K_i^{*T} x(t) + L_i^* r(t) + M_i^*) + f_i = A_{mi} x(t) + B_{mi} r(t) + f_{mi}, t \geq 0, \tag{3-19}$$

has a uniformly bounded solution $x(t)$. The above control law leads to the tracking error dynamics $\dot{e} = A_m(t)e(t)$, where $e(t) = x(t) - x_m(t)$. The error $e(t)$ converges to zero exponentially if T_0 satisfies the condition (3-6).

Nonetheless, In most of the practical applications the plant parameter matrices A_i and B_i were unknown and hence, nominal control law (3-17) can not be carried out to achieve closed loop stability. In this case, the adaptive control structure used was as follows:

$$u(t) = K^T(t)x(t) + L(t)r(t) + M(t) \tag{3-20}$$

where,

$$K(t) = \sum_{i=1}^{l} K_i(t) \chi_i(t) \qquad L(t) = \sum_{i=1}^{l} L_i(t) \chi_i(t) \qquad M(t) = \sum_{i=1}^{l} M_i(t) \chi_i(t) \tag{3-21}$$

The closed loop system structure was shown in Figure 3-2

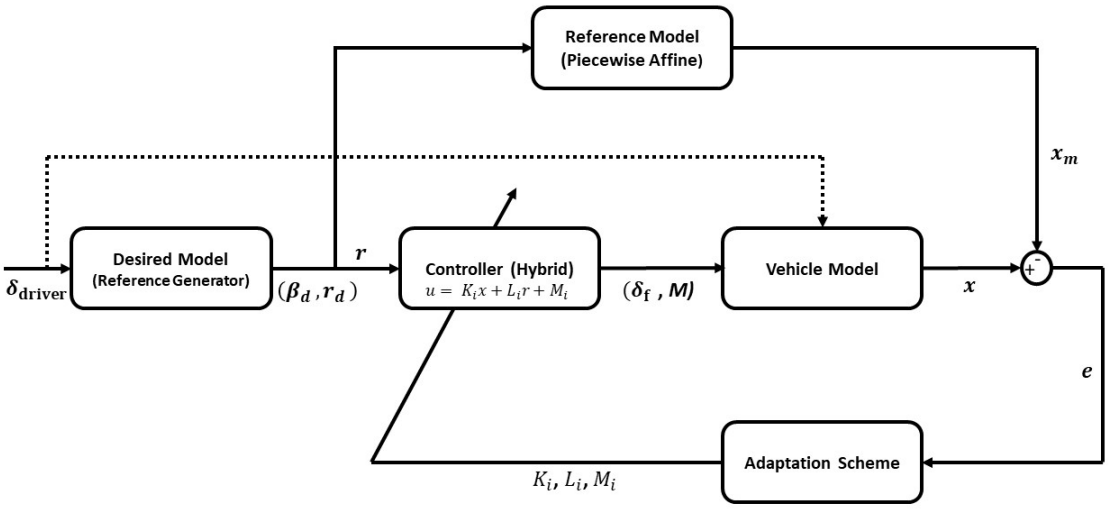

Figure 3-2: Application of proposed control scheme to vehicle model

In this case, the controller gains K^*, L^* and M^* can not be implemented directly and must be estimated. Using time-varying estimates of the nominal controller parameters in (3-21) and system dynamics in (3-1).

$$\begin{aligned}\dot{x}(t) &= A_i x(t) + B_i(K^T(t)x(t) + L(t)r(t) + M(t)) + f_i \\ &= A_{mi}x(t) + B_{mi}r(t) + B_i(\tilde{K_i}^T x(t) + \tilde{L_i}(t)r(t) + \tilde{M_i}(t)) \\ &= A_{mi}x(t) + B_{mi}r(t) + B_{mi}(L_i^{*-1}\tilde{K_i}^T x(t) + L_i^{*-1}\tilde{L_i}(t)r(t) + L_i^{*-1}\tilde{M_i}(t))\end{aligned} \tag{3-22}$$

Further it leads to the tracking error model:

$$\dot{e} = \dot{x} - \dot{x_m} = \sum_{i=1}^{l}(A_{mi}\chi_i e + B_{mi}L_i^{*-1}\chi_i(\tilde{K_i^T}x + \tilde{L_i}r + \tilde{M_i})) \tag{3-23}$$

where $\tilde{K_i^T}(t) = K_i^T(t) - K_i^{*T}$, $\tilde{L_i}(t) = L_i(t) - L_i^*$ and $\tilde{M_i}(t) = M_i(t) - M_i^*$, $i \in I$ were the errors accounted in the controller parameter estimates.

Adaptation mechanism / Adaptive laws

The error model defined in (3-23) was used to develop the adaptive laws. Considering the case when a common Lyapunov matrix exists for the constituent reference model A_{mi}

Adaptation law used in existence of common Lyapunov matrix P_m Since in reference model (3-4) the matrices A_{mi} were Hurwitz, $i \in I$. So, in order to generate a bounded signal state x_m from bounded r, there should exist a common positive definite Lyapunov matrix $P_m = P_m^T > 0$, such that the following inequality holds:

$$A_{mi}^T P_m + P_m A_{mi} < 0 \tag{3-24}$$

The adaptive laws which were proposed to ensure the stability of the closed loop system were as follows:

$$\begin{aligned}\dot{K_i^T}(t) &= -S_i^T B_{mi}^T \chi_i(t) P_m e(t) x^T(t) \\ \dot{L_i}(t) &= -S_i^T B_{mi}^T \chi_i(t) P_m e(t) r^T(t) \\ \dot{M_i}(t) &= -S_i^T B_{mi}^T \chi_i(t) P_m e(t)\end{aligned} \tag{3-25}$$

This type of adaptive control scheme should follow the following stability and tracking properties:
Theorem 3-2.2. *[33]. If the parameter matrices A_{mi}, $i \in I$ for the reference model system* (3-4) *satisfies the inequality* (3-24) *and there exist a common lyapunov matrix P_m such that, $P_m = P_m^T > 0$. This allows all the signals in closed loop system to remain bounded and state tracking error $e(t) = x(t) - x_m(t)$ to converge asymptotically to* 0*, even for the arbitrarily fast switching.*

Proof. Let $A_{mi}^T P_m + P_m A_{mi} = -Q_{mi}$ for $Q_{mi} = Q_{mi}^T > 0$ (positive definite) for $i \in I$. In order to establish the stability, the candidate Lyapunov function considered is as follows:

$$V = e^T P_m e + \sum_{i=1}^{l} (tr[\tilde{K}_i G_i^{-1} \tilde{K}_i{}^T] + tr[\tilde{L}_i{}^T G_i^{-1} \tilde{L}_i] + tr[\tilde{M}_i{}^T G_i^{-1} \tilde{M}_i]) \tag{3-26}$$

where G_i is from (3-15)

For matrices $K(t)$, $L(t)$ and $M(t)$ the state vector of the closed loop system is

$$e_c(t) = [e^T(t), \tilde{K}^T(t), \tilde{L}(t), \tilde{M}(t)]$$

$$\tilde{K}_i{}^T(t) = [\tilde{k}_{i1}, \tilde{k}_{i2}, ..., \tilde{k}_{in}] \qquad \tilde{L}_i(t) = [\tilde{l}_{i1}, \tilde{l}_{i2}, ..., \tilde{l}_{im}] \qquad \tilde{M}_i(t) = [\tilde{m}_{i1}, \tilde{m}_{i2}, ..., \tilde{m}_{iq}] \tag{3-27}$$

and $tr[.]$ denoting the trace of the square matrix. Under the (2) and with the certainty that the $tr[G_1 G_2] = tr[G_2 G_1]$, $tr[G_3] = tr[G_3^T]$, for any matrices G_i $i = 1,2,3$ of appropriate dimensions, its time derivative along the adaptive laws (3-25) is,

$$\begin{aligned} \dot{V} &= \dot{e} P_m e^T + e^T P_m \dot{e} + 2tr[\tilde{K}_i G_i^{-1} \dot{\tilde{K}}_i^T] + 2tr[\tilde{L}_i{}^T G_i^{-1} \dot{\tilde{L}}_i] + 2tr[\tilde{M}_i{}^T G_i^{-1} \dot{\tilde{M}}_i]) \\ &= e^T [A_{mi}^T P_m + P_m A_{mi}] e + 2e^T P_m B_{mi} L_i^{*-1} \tilde{K}_i^T x + 2e^T P_m B_{mi} L_i^{*-1} \tilde{L}_i r + 2e^T P_m B_{mi} L_i^{*-1} \tilde{M}_i \end{aligned} \tag{3-28}$$

Now using the trace conditions and the adaptive laws (3-25) we have:

$$\dot{V} \leq -(\min_{i \in I} \lambda_{\min}[Q_{mi}]) ||e||^2 \tag{3-29}$$

It pursues that $e(t) \in \mathscr{L}_2 \cap \mathscr{L}_\infty$, $K_i(t)$,$L_i(t)$ and $M_i(t) \in \mathscr{L}_\infty$ with $x_m(t) \in \mathscr{L}_\infty$ (see Remark (3-2.1)), $u(t)$, $\dot{e}(t) \in \mathscr{L}_\infty$. Hence, all signals are bounded in closed-loop system. According to Barbalat's Lemma, $lim_{t \to \infty} e(t) = 0$. □

Usually, certain particular sets of matrices in the special structure have a common P_m matrix. If no common Lyapunov matrix exists than special structure of adaptive laws are adopted.

Remark 3-2.3. *If the common positive definite matrix P_m exists such that Lyapunov inequality is satisfied, then the switched system is globally asymptotically stable for arbitrary switching (arbitrary slow or fast switching). The condition required for the existence of common positive definite matrix P_m is that the system matrices can be simultaneously be triangularized using a non-singular transformation T. The details are discussed in [39]*

Adaptation law used when no common Lyapunov matrix P_m exist Satisfying the Lyapunov inequality (3-24) when no common Lyapunov matrix P_m exists for the set of the stable matrices A_{mi}, $i \in I$, the parameter projection adaptive laws were applied, with certain assumption of the lower and upper bounds on the controller parameters. These adaptive laws were as follows:

$$\begin{aligned}\dot{K}_i^T(t) &= -S_i^T B_{mi}^T \chi_i(t) P_m e(t) x^T(t) + F_{K_i}(t)\\ \dot{L}_i(t) &= -S_i^T B_{mi}^T \chi_i(t) P_m e(t) r^T(t) + F_{L_i}(t)\\ \dot{M}_i(t) &= -S_i^T B_{mi}^T \chi_i(t) P_m e(t) + F_{M_i}(t)\end{aligned} \tag{3-30}$$

The adaptive laws in (3-30) were required to update the parameters of the controller structure (3-20). For this control design, the parameter projection terms were effective with assumption.
Assumption 4. *The known constant matrix S_i is such that $G_i = L_i^* S_i$ is diagonal and positive definite.*

The choice on the initial estimates of each element in $K(t)$, $L(t)$ and $M(t)$ was chosen within the known bounds. The parameter estimates were confined within these bounds at all times by using the parameter projection terms $F_{K_i}(t)$, $F_{L_i}(t)$, $F_{M_i}(t)$. The parameter adaptation was allowed to be active when the estimates lie within these bounds, otherwise, the adaptation deactivates, and estimates remain unchanged for that period of time (i.e. $\dot{K}_i(t) = 0, \dot{L}_i(t) = 0, \dot{M}_i(t) = 0$). Evolution of estimates of these gains with time can be seen in Figure 3-3

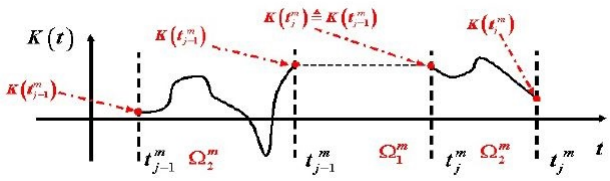

Figure 3-3: A generic evolution of controller gain $K(t)$ [6]

The stability and tracking properties are followed by the system using the definitions in *Lemma* (3-6) and the following theorem follows:
Theorem 3-2.3. *[33]. The controller structure* (3-20) *updated by the adaptive laws* (3-30) *have all the closed loop signals bounded with a small tracking error in the sense that;*

$$\int_t^{t+T} e(\tau)^T e(\tau) d\tau \leq \mu \Delta_{A_m} c_0 \frac{T}{T_0} + c_1, \qquad t \geq t_0, \qquad T > 0 \tag{3-31}$$

such that $c_1 = (1 + \mu\Delta_{A_m}) c_0$ for some $c_0 > 0$

3-3 Summary

The work established in this chapter provides a novel adaptive control approach that ensures the asymptotic tracking for the switched affine system. This policy was able to handle the parameter uncertainties and known input disturbances. It used a Lyapunov-based approach for deriving the adaptive mechanism in order to adjust the control parameters. The derived hybrid control policy based on error tracking model hence guarantee the global asymptotic stability and state-tracking. The practical implementation was done on the PWA vehicle model in order to indicate the effectiveness of the proposed hybrid adaptive control scheme.

Chapter 4

Simulation Results and Discussion

This chapter is organized as follows: In Section 4-1 to demonstrate the stability properties, tracking performance and effectiveness of the hybrid adaptive policy employed as the integrated chassis control groundwork has been designed. The studied control methodology was then implemented using the software MATLAB/Simulink and was verified via simulations. In Section 4-2 the simulations were performed on the PWA vehicle model as proposed in (2-11). The subsections in 4-2 ensure the robustness of the controller against the uncertainties in vehicle speed and the variation in the tire parameters. Section 4-4 includes the validation of the controller on the nonlinear model.

The integrated control was designed and tuned at standard test vehicle velocity of 20 m/s. The controller was able to give two independent control signals to the vehicle model in the form of steering angle and yaw moment. The effectiveness of the controller was exhibited by using various experiments which include the closed loop steering test to examine the closed loop system behavior.

The closed loop test includes the following:

- Test to check the robustness against the variations in the parameters of the system (the tire parameters were updated describing the change in friction coefficient).
- Test to check robustness against variation in vehicle speed.
- Test to check the fault tolerance capabilities of the active safety system.
- Test to check the efficiency of the system against the disturbances employed by the driver in the form of steering and braking (hard braking by using hand-brake scenario was discussed later in the thesis).

4-1 Design and simulation parameters

The PWA vehicle system (3-1) was used to check the effectiveness of hybrid adaptive control policy. The most important step was to design the stable reference model. A reference model subsystem

was chosen to determine the desired behavior of the vehicle. The reference model will take the form as defined in (3-4). The reference trajectories within the neighborhood of the corresponding steady states in different PWA regions were pieced together forming a global reference trajectory to specify a piecewise reference model.

In order to achieve the control objectives, the Assumptions (1),(2),(3) specified in the design conditions must be fulfilled. This was ensured by using the nominal affine closed loop system dynamics as the reference model system. Primarily, the linear quadratic controller (LQ) of the form of $u_{nominal} = K_i^{*T} x(t) + L_i^* r(t) + M_i^*$ was designed based on the knowledge of the (A_i, B_i).

The state feedback gains K_i^* were chosen by using a linear quadratic state feedback regulator designed to achieve the stabilization and asymptotic tracking of yaw rate (r), which minimize the cost function of the form:

$$J = \int_0^\infty (xQx^T + u^T Ru)\,dt \tag{4-1}$$

where the weighing matrices were defined as:

$$Q_1 = Q_3 \begin{bmatrix} 100 & 0 \\ 0 & 100 \end{bmatrix} \qquad Q_2 = \begin{bmatrix} 10 & 0 \\ 0 & 10 \end{bmatrix}$$

$$R_1 = R_2 = R_3 \begin{bmatrix} 15 & 0 \\ 0 & 15 \end{bmatrix}$$

The feedforward gains L_i^* were chosen to be $L_i^* = -(C_i A_{mi}^{-1} B_i)^{-1}$, such that the diagonal elements of the transfer matrix $\Gamma(s) = C_i(sI - A_{mi})^{-1} B_i L_i^*$ have DC gain equal to one, at the same time the off diagonal elements of the transfer matrix have zero DC gain, such that $\Gamma(s) = I_n$ and gains M_i^* were chosen based on Assumption (3). It was important to highlight that the matrices (A_i, B_i) were available for the simulation process. But the controller design does not use the knowledge of these matrices, on the other hand only the knowledge of the reference model parameter matrices were used. The matrices S_i were chosen based on Assumption (2) such that gains G_i were symmetric and positive definite. The gains G_i chosen were as follows:

$$G_1 = G_3 \begin{bmatrix} 100 & 0 \\ 0 & 100 \end{bmatrix} \qquad G_2 = \begin{bmatrix} 20 & 0 \\ 0 & 20 \end{bmatrix}$$

Remark 4-1.1. *For the arbitrary S_i satisfying the Assumption* (2) *the closed loop stability and tracking performance was attained as stated in Chapter 3. These matrices were the adaptation gain matrices which were adjusted to achieve the desired adaptation rate. In general, if gains S_i were large, then the controller was able to make faster adaptations and hence gives better performance. But, sometimes the fast adaptation may lead to system destabilization due to high frequency transients and unmodeled dynamics of the system. So, in order to choose the gains S_i in practice, the system performance has to be observed in the simulations.*

It was also important to obtain the Lyapunov matrices for the adaptive laws to work. For the existing system a common Lyapunov matrix existed which was obtained by solving the following $LMI's$.

$$\begin{aligned} P_m &> 0 \\ A_{m1}^T P_m + P_m A_{m1} &< 0 \\ A_{m2}^T P_m + P_m A_{m2} &< 0 \\ A_{m3}^T P_m + P_m A_{m3} &< 0 \end{aligned} \tag{4-2}$$

The common Lyapunov matrix obtained was as follows:

$$P_m = \begin{bmatrix} 7.1950 & -0.3469 \\ -0.3469 & 1.0194 \end{bmatrix}$$

with the positive eigenvalues $\begin{bmatrix} 1 & 7.2144 \end{bmatrix}$. It was observed that the matrix P_m obtained was symmetric and positive definite by solving the above $LMI's$ (4-2). The ideal controller gains calculated were made available in Appendix C.

4-2 Simulation results: Closed-loop steering Test

The simulations were performed on the software package MATLAB/Simulink and the following tests were carried out on the vehicle model to present the functionality and robustness of the hybrid adaptive control policy.

4-2-1 System performance with varying vehicle speed

In this section, the hybrid adaptive integrated policy (where AFS and ESP were working together) was tested with the controller in the loop with the Sine with Dwell steering at the range of the coasting speeds varying from 15 m/s to 25 m/s. Since the hybrid adaptive controller was designed and tuned at the speed of 20 m/s, testing it with the variations in longitudinal velocity can guarantee the robustness of the system to the uncertainties in velocity of the vehicle. The performance was also observed in the presence of the individual safety systems when the AFS and ESP were working individually or in the other sense, it can be seen as the system performance during a particular system failure. Demonstrating how well the system can recover during the braking system failure (ESP failure) when the only working actuator was steering or vice-versa. The comparison in the performance of the system was observed without re-tuning the controller.

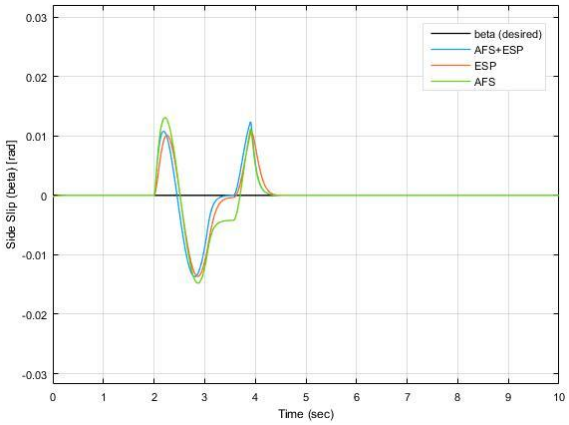

(a) Side slip angle

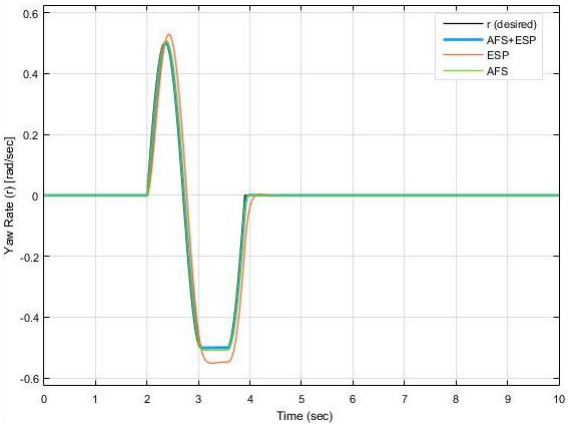

(b) Yaw rate

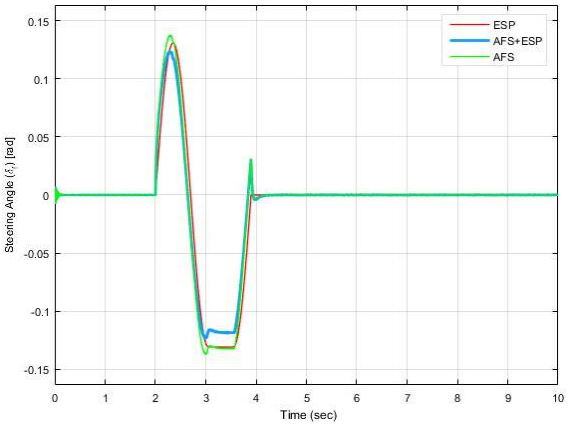

(c) Steering angle

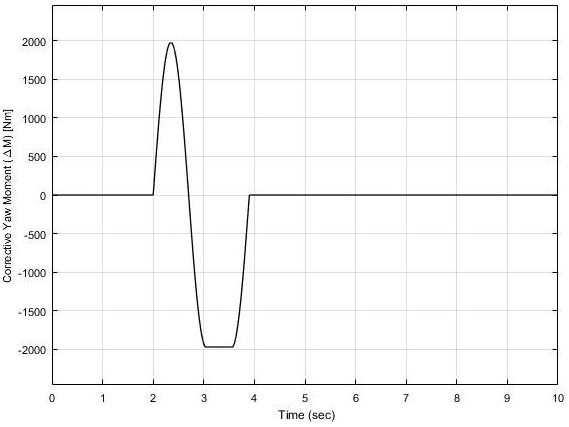

(d) Yaw moment

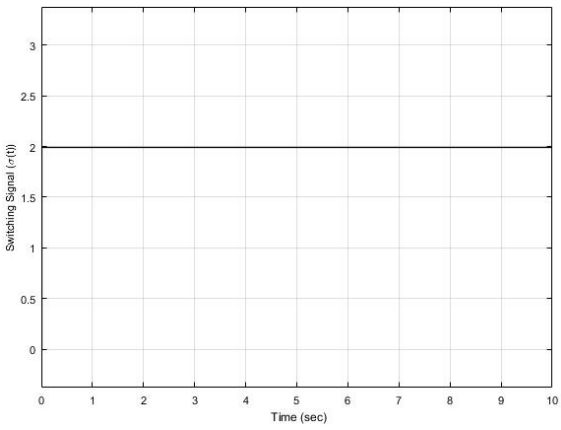

(e) Switching signal

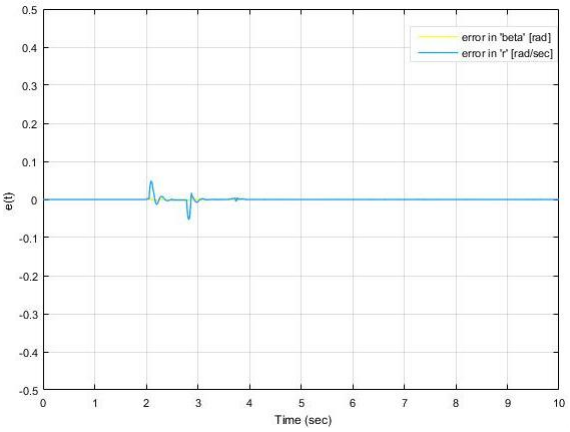

(f) Tracking error

Figure 4-1: Simulation results for SWD maneuver coasting at $15 m/s$

Simulations were obtained by keeping the longitudinal velocity constant to $15 m/s$. At this longitudinal velocity, the vehicle stays in the linear region. The side slip angle of the vehicle was bounded and the controller was able to track the reference yaw rate.

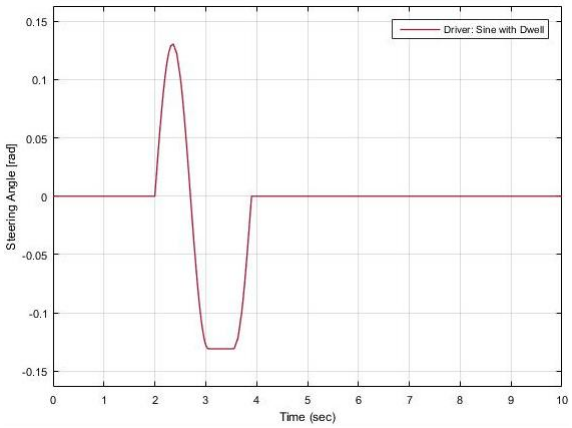

(a) Steering angle by driver

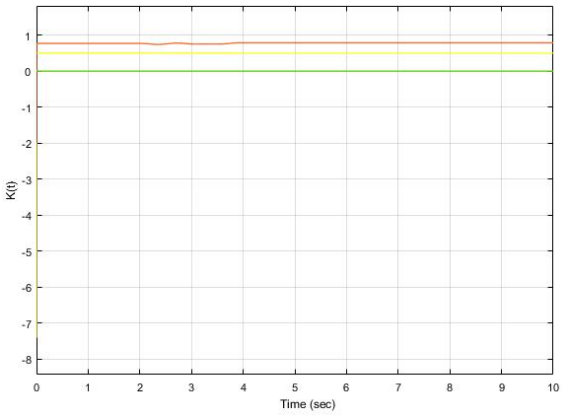

(b) Estimate of controller gain $(K(t))$

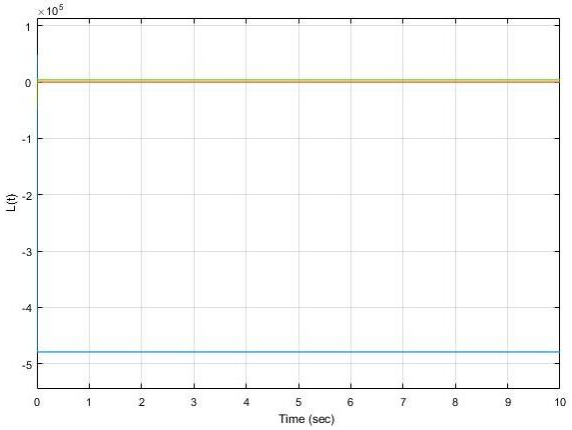

(c) Estimate of controller gain $(L(t))$

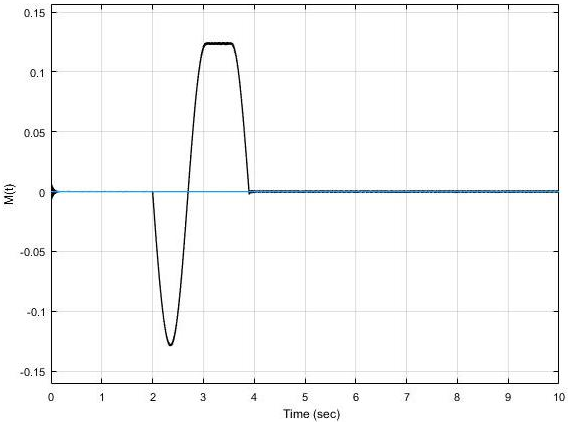

(d) Estimate of controller gain $(M(t))$

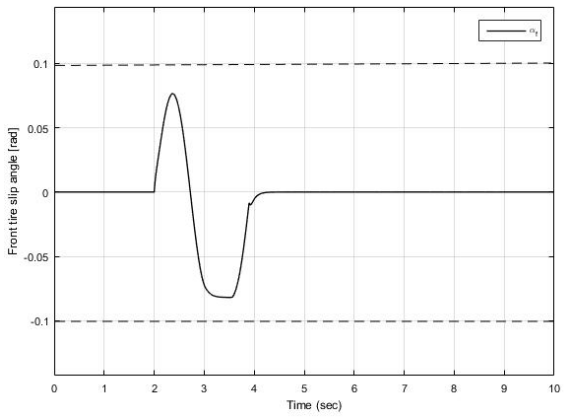

(e) Front tire slip angle (α_f)

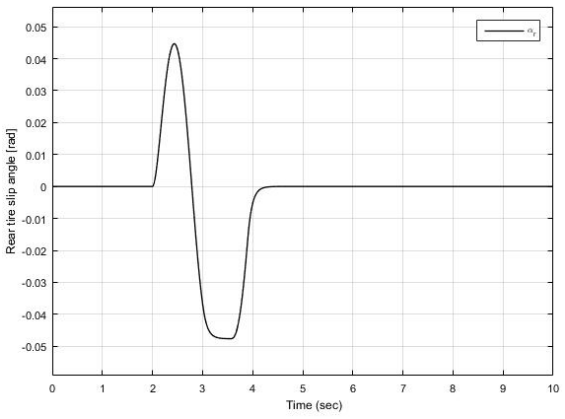

(f) Rear tire slip angle (α_r)

Figure 4-2: Simulation results for SWD maneuver coasting at $15m/s$

The slip angle of front tire saturates before the rear tire. Particularly in this case the front tire does not reach the saturation limit and vehicle dynamics remain in the linear region and switching does not occur. The switching signal was active in $Region\ 2$ for the complete simulation.

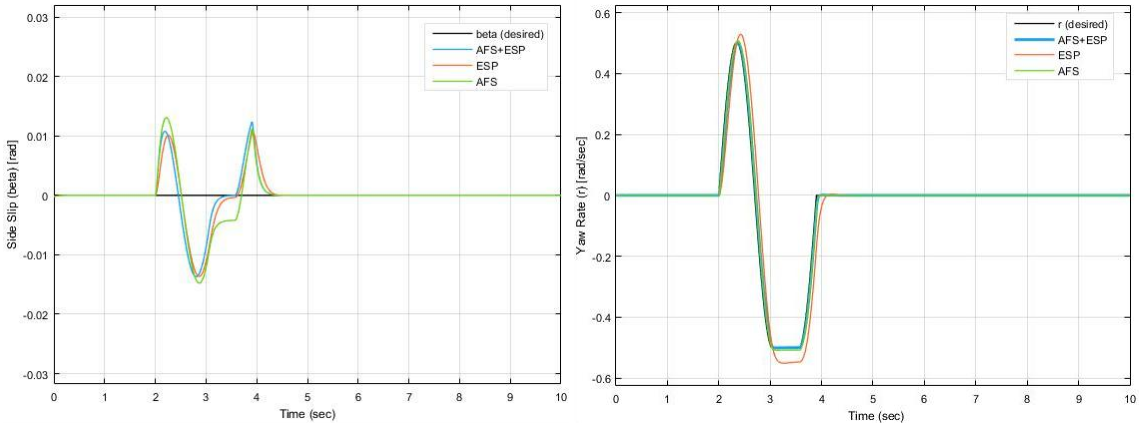

(a) Side slip angle (Linear control) **(b)** Yaw rate (Linear control)

Figure 4-3: Simulation results for SWD maneuver coasting at 15m/s with linear control only

While coasting at the constant longitudinal velocity of $15 m/s$ the vehicle response were obtained in the simulations shown in Figure 4-1 to Figure 4-3. The observations made were as follows:

- The vehicle coasting at the longitudinal velocity of $15 m/s$ stays in the linear region ($Region$ 2), can be seen in Figure 4-1e. The front tire slip angle (α_f) stays within the saturation limit of 0.101 rad in Figure 4-2e, which does not allow the switching to occur.
- All three control algorithms were able to ensure the lateral stability of the vehicle when the hybrid adaptive control policy was active. The side slip angle was bounded close to zero with a peak angle of 0.013 rad and yaw rate was tracking the desired trajectory smoothly with a peak of 0.5 rad/sec, and a small overshoot was observed when only ESP was working.
- The best reference tracking was obtained with the integration of the both safety systems ($AFS + ESP$) i.e when both control inputs δ_f and ΔM were active.
- The two control inputs required to stabilize the system, i.e. the front tire steering angle (δ_f) and the yaw moment (ΔM) were shown in Figure 4-1c and Figure 4-1d respectively.
- As observed from Figure 4-3, the linear controller was able to give the equivalent stable response as compared to, when the hybrid adaptive controller was working. This type of response was expected as nonlinear dynamics were not excited at this particular velocity.

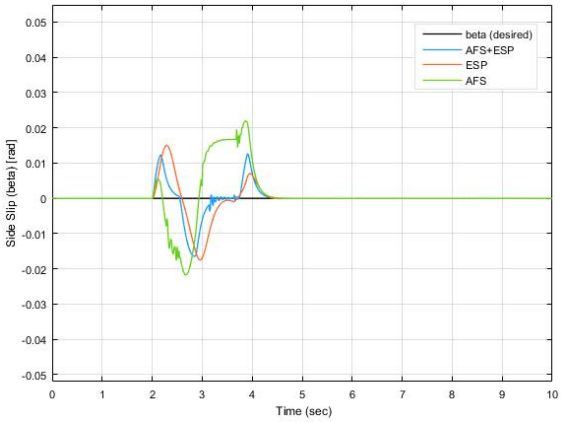

(a) Side slip angle

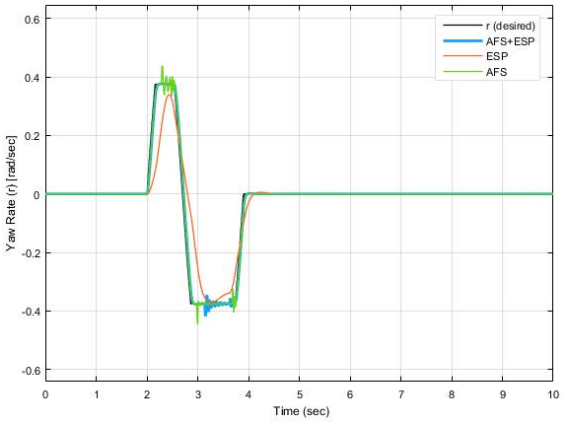

(b) Yaw rate

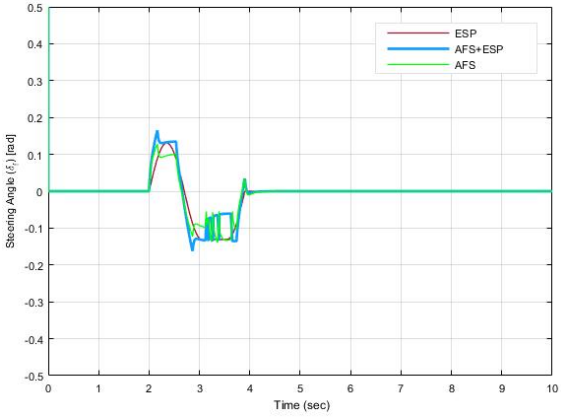

(c) Steering angle

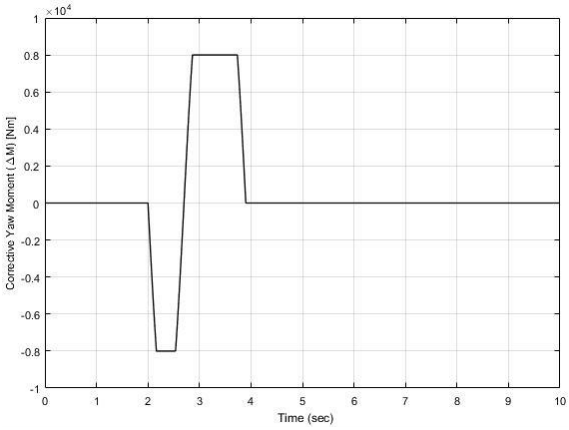

(d) Yaw moment

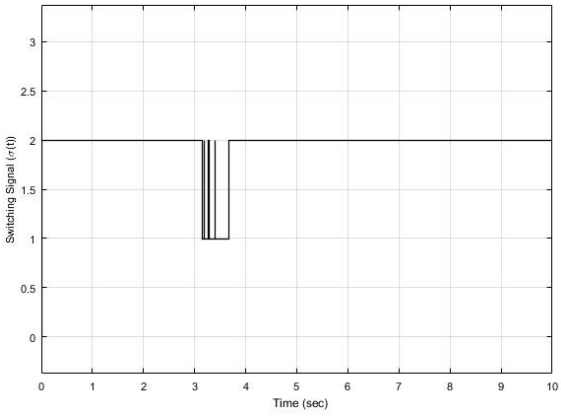

(e) Switching signal

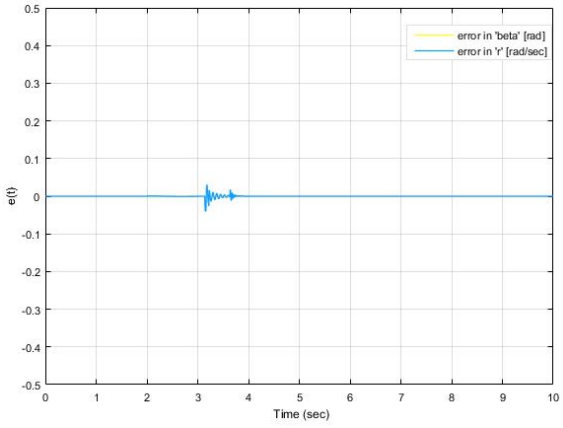

(f) Tracking error

Figure 4-4: Simulation results for SWD maneuver coasting at $20m/s$

These simulations were obtained by keeping the longitudinal velocity constant to $20m/s$. At this longitudinal velocity, the vehicle enters the nonlinear region. The side slip angle of the vehicle was bounded and the controller was able to track the reference yaw rate.

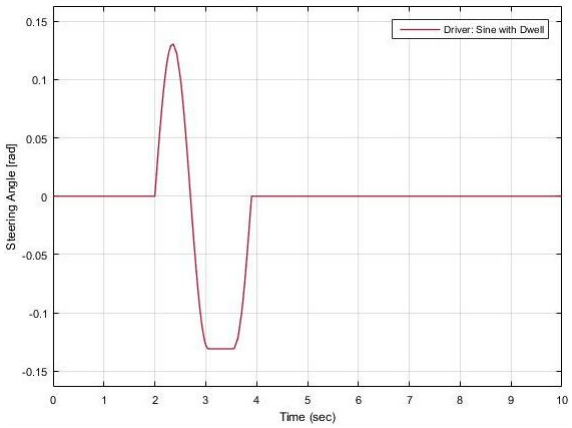

(a) Steering angle by driver

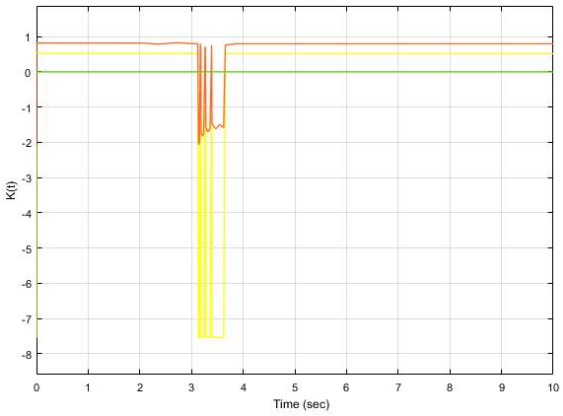

(b) Estimate of controller gain $(K(t))$

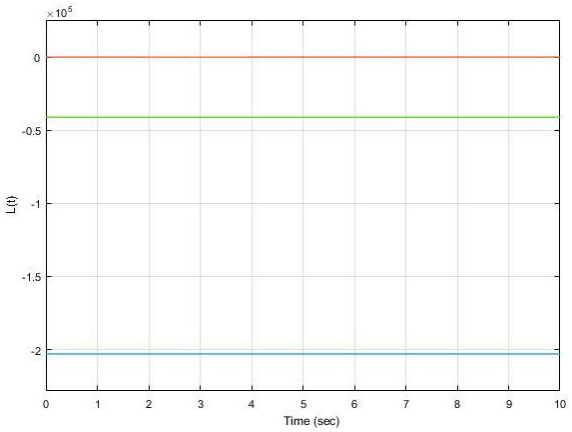

(c) Estimate of controller gain $(L(t))$

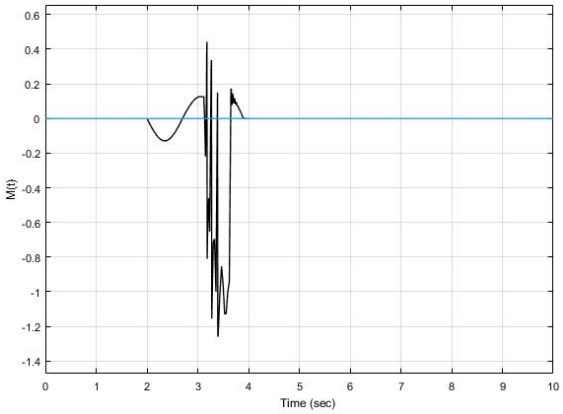

(d) Estimate of controller gain $(M(t))$

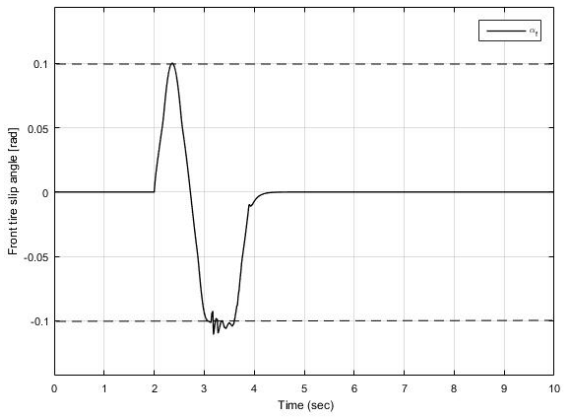

(e) Front tire slip angle (α_f)

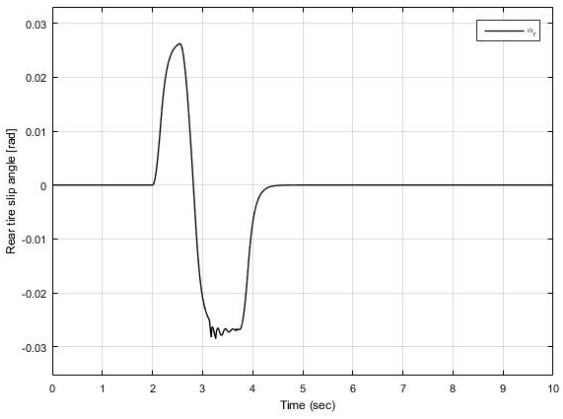

(f) Rear tire slip angle (α_r)

Figure 4-5: Simulation results for SWD maneuver coasting at $20m/s$

The slip angle of front tire saturates before the rear tire. The front tire slip angle works outside the linear region in this case and allows the switching to occur. With the evolution of front tire slip angle, the switching signal was active in $Region\ 1$ and $Region\ 2$.

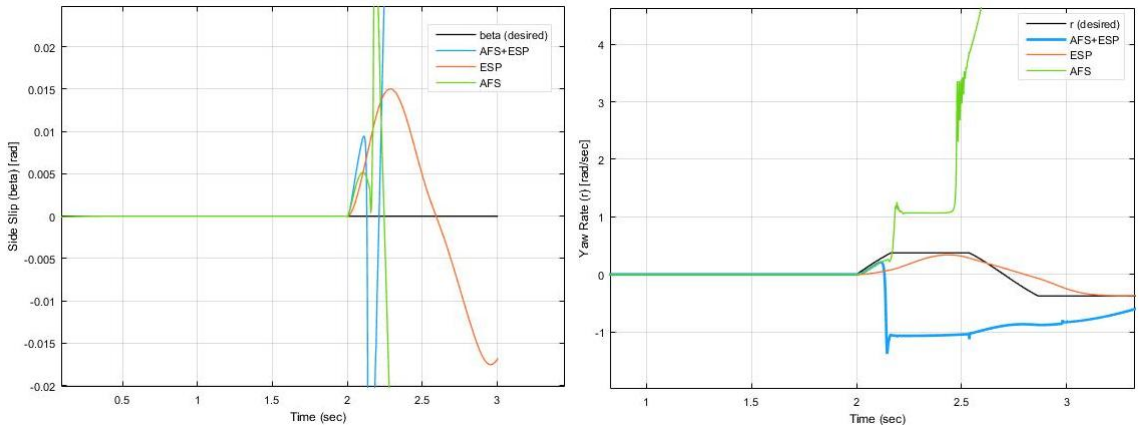

(a) Side slip angle (Linear control) **(b)** Yaw rate (Linear control)

Figure 4-6: Simulation results for SWD maneuver coasting at 20m/s with linear control only

The observations made from the Figure 4-4 to Figure 4-6 when the vehicle was coasting at constant longitudinal velocity of $20 m/s$ were as follows:

- The vehicle coasting at the longitudinal velocity of $20 m/s$ was able to excite the nonlinear characteristics of the system. This can be observed by the switching signal in Figure 4-4e. The front tire slip angle (α_f) reach the saturation limit of 0.101 rad and allows the switching to occur. This can be seen in Figure 4-5e.
- All three control algorithms try to achieve the lateral stability of the vehicle when the hybrid adaptive control policy was active. The side slip angle was bounded close to zero with a peak angle of 0.013 rad and yaw rate was tracking the desired trajectory smoothly with a peak of 0.385 rad/sec.
- The best reference tracking was obtained with the integration of the both safety systems ($AFS + ESP$) i.e. when both control inputs δ_f and ΔM were active.
- The two control inputs required to stabilize the system, i.e. the front tire steering angle (δ_f) and the yaw moment (ΔM) were shown in Figure 4-4c and Figure 4-4d respectively.
- The estimates of the controller parameters which allows the adaptation of the hybrid controller to follow the reference trajectory were shown in Figure 4-5.
- The norm of state tracking error can be observed in Figure 4-4f.
- As observed from Figure 4-6, with only the linear controller in action the system response became poor when compared to a working hybrid adaptive controller. The linear controller was not able to bound the side slip angle and yaw rate of the vehicle, leading the vehicle to go into a spin. On the other hand, the hybrid adaptive control meets the performance specifications required for stability and allows the vehicle to follow the desired trajectory.

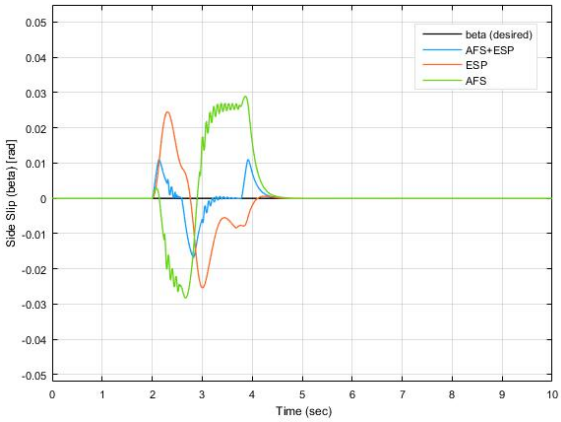

(a) Side slip angle

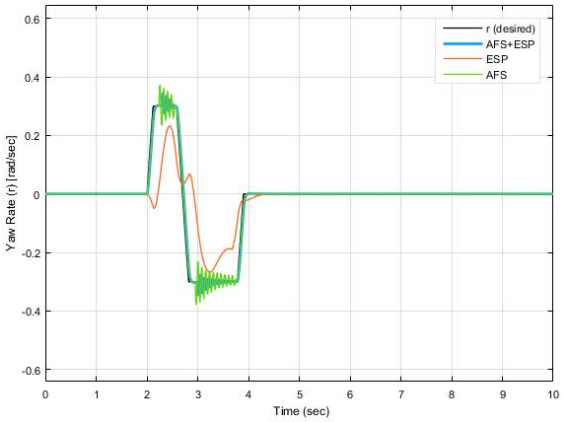

(b) Yaw rate

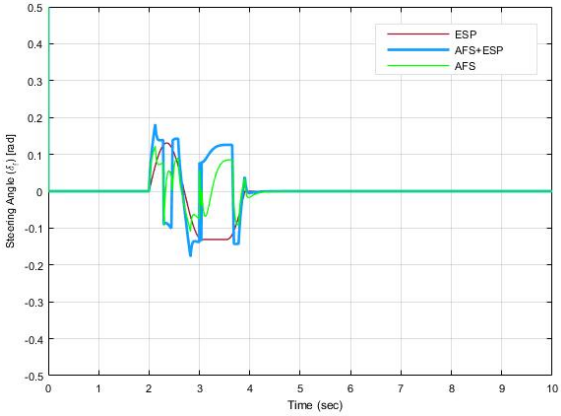

(c) Steering angle

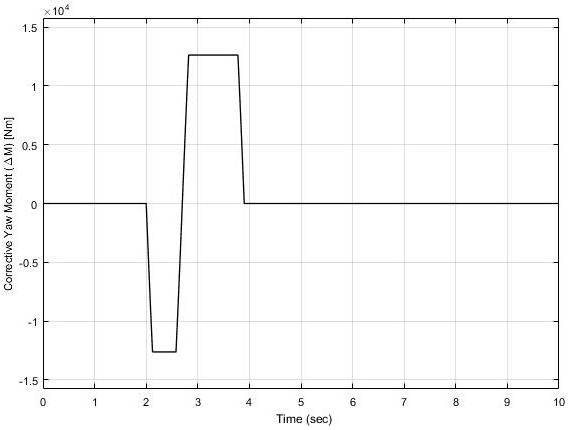

(d) Yaw moment

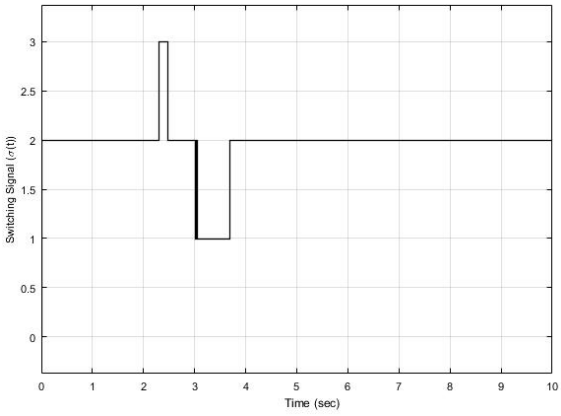

(e) Switching signal

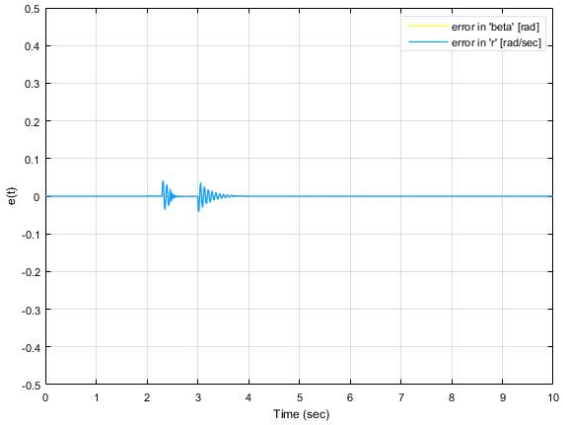

(f) Tracking error

Figure 4-7: Simulation results for SWD maneuver coasting at $25 m/s$

The simulations above were obtained by keeping the longitudinal velocity constant to $25 m/s$. At this longitudinal velocity, the vehicle enters the nonlinear region. The side slip angle of the vehicle was bounded and the controller was able to track the reference yaw rate.

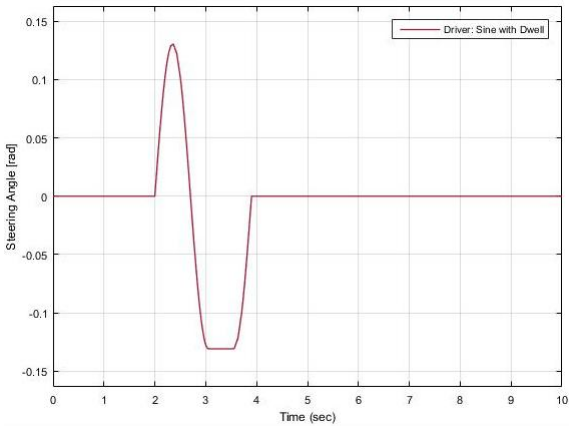

(a) Steering angle by driver

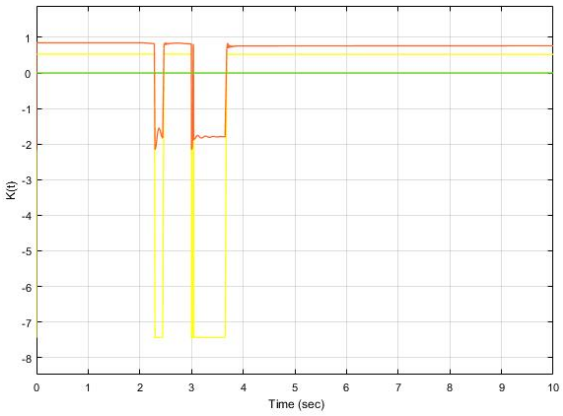

(b) Estimate of controller gain $(K(t))$

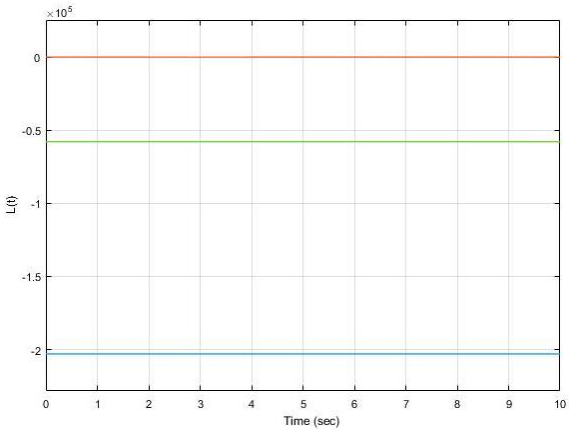

(c) Estimate of controller gain $(L(t))$

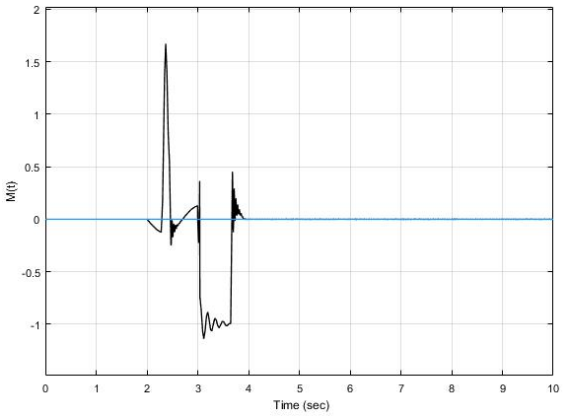

(d) Estimate of controller gain $(M(t))$

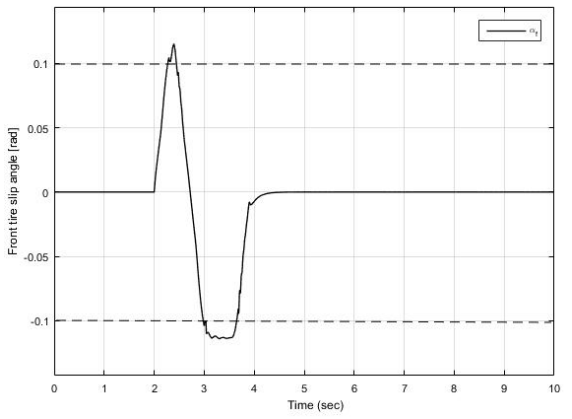

(e) Front tire slip angle (α_f)

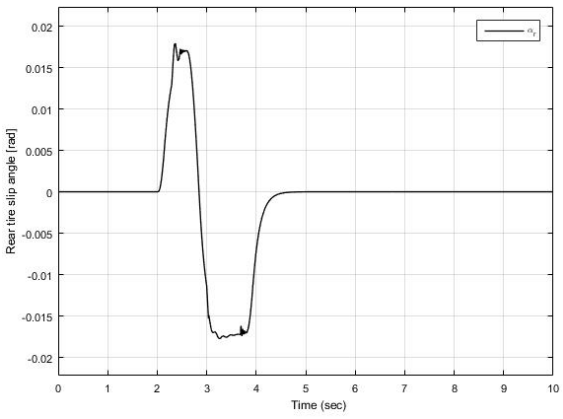

(f) Rear tire slip angle (α_r)

Figure 4-8: Simulation results for SWD maneuver coasting at $25m/s$

The slip angle of front tire saturates before the rear tire and the vehicle was operated in the non-linear region. With the evolution of front tire slip angle, the switching signal was active in different regions.

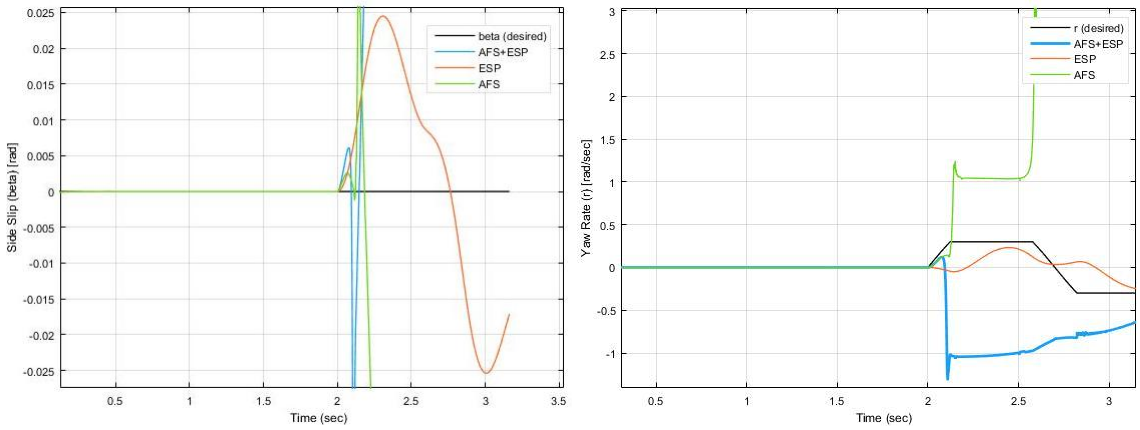

(a) Side slip angle (Linear control) **(b)** Yaw rate (Linear control)

Figure 4-9: Simulation results for SWD maneuver coasting at 25m/s with linear control only

The observations made from the simulation results, when the vehicle was coasting at constant longitudinal velocity of $25 m/s$ from the Figure 4-7 to Figure 4-9 were as follows:

- The vehicle coasting at the longitudinal velocity of $25 m/s$ was able to excite the nonlinear characteristics of the system. This can be observed by the switching signal in Figure 4-7e. The front tire slip angle (α_f) reach the saturation limit of 0.101 rad and allow the switching to occur. This can be seen in Figure 4-8e.
- All three control algorithms try to achieve the lateral stability of the vehicle when the hybrid adaptive control policy was active. The side slip angle was bounded close to zero with a peak angle of 0.02 rad and yaw rate was tracking the desired trajectory smoothly with a peak of 0.3 rad/sec.
- The best reference tracking was obtained with the integration of the both safety systems ($AFS + ESP$) i.e when both control inputs δ_f and ΔM were active.
- The two control inputs required to stabilize the system, i.e. the front tire steering angle (δ_f) and the yaw moment (ΔM) were shown in Figure 4-7c and Figure 4-7d respectively.
- The estimates of the controller parameters which allows the adaptation of the hybrid controller to follow the reference trajectory were shown in Figure 4-8.
- The norm of state tracking error can be observed in Figure 4-7f.
- As observed from Figure 4-9, with only the linear controller in action the system response became poor when compared to the hybrid adaptive controller in working. The linear controller was not able to bound the side slip angle and yaw rate of the vehicle, leading vehicle to go into the spin. On the other hand, the hybrid adaptive control meets the performance specifications and allows the vehicle to follow the desired trajectory.

It can be observed from the three cases discussed above to check the robustness to vehicle velocity, better system performance was obtained with the hybrid adaptive policy. The lateral stability was achieved at higher velocities by compensating with the small yaw rate and relatively large side slip angle of the vehicle. Also, the ESP stability criteria discussed in (2-15) and (2-16) were both satisfied by the hybrid adaptive control scheme and hybrid ICC passed the test. On the other hand

the linear ICC failed the test based on the similar criterion which failed to bound the side slip angle and yaw rate of the vehicle. The closed-loop system performance was compared in Table 4-1 and was observed that the hybrid adaptive ICC performance was best in terms of penalizing the peak overshoot in the system states.

Table 4-1: Closed-loop system performance: Comparison

Speed ⇒	15 m/s		20 m/s		25 m/s	
Safety System ⇓	β overshoot (%)	r overshoot (%)	β overshoot (%)	r overshoot (%)	β overshoot (%)	r overshoot (%)
AFS	1.3	4	2.2	9.09	2.9	28.33
ESP	1.1	12	1.5	−3.8	2.4	−23.45
AFS + ESP	1.1	2	1.05	6.5	1	8.2

It was observed from Table 4-1, that the closed-loop system performance of all three control algorithm gave better performance compared to the open-loop system performance as described in Table 2-2, but the best system performance was observed with ICC (AFS+ESP) in the loop. The ICC was able to penalize the overshoot in r from 52.64% to 6.5% for the vehicle coasting at test speed of 20m/s. Here, the negative sign of the magnitude represents undershoot.

4-2-2 System performance with varying tire parameters

The Hybrid Adaptive Policy for the reference tracking of side slip angle and yaw rate of the vehicle was also tested for the robustness to the variation in the tire parameters. The different test case was assumed with the different piecewise tire parameters expressing the tire behavior when the vehicle was moving on the soil (when the friction was less) instead of the asphalt as in the previous case (when the friction was high). The front tire saturation limit $\hat{\alpha_f} = 0.07\ rad$ was chosen in this case. The parameters used in this test case were provided in Appendix B. While testing the controller on the different tire parameters the controller was not re-tuned. These parameters were also tested for the robustness to vehicle velocity varying from $15m/s$ to $25m/s$ while using the same controller parameters used in the previous case, which was tuned at vehicle velocity of $20m/s$. The vehicle at the velocity of the $15m/s$ does not excite the nonlinearities and a similar kind of tracking was obtained as was obtained with the parameters used previously. The simulations were plotted. The results obtained from the hybrid adaptive strategy in working were obtained as follows:

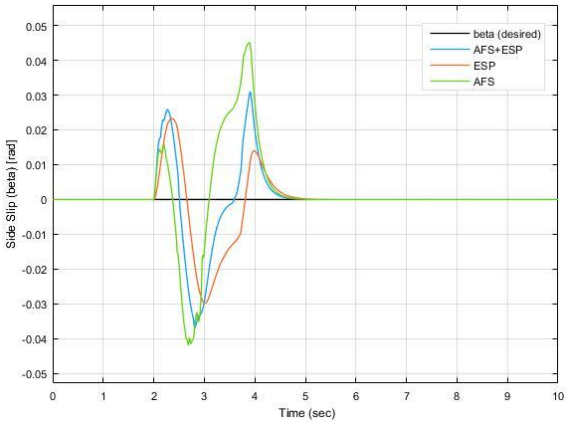

(a) Side slip angle

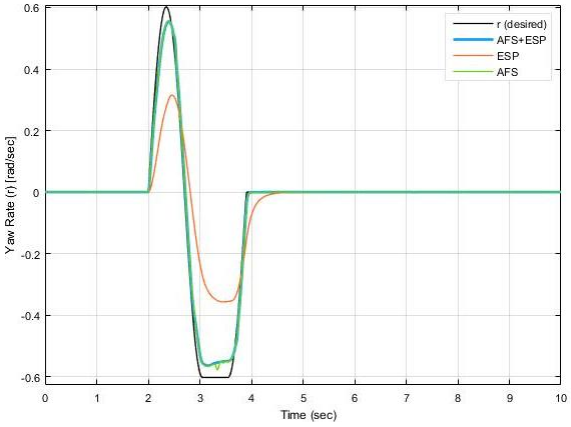

(b) Yaw rate

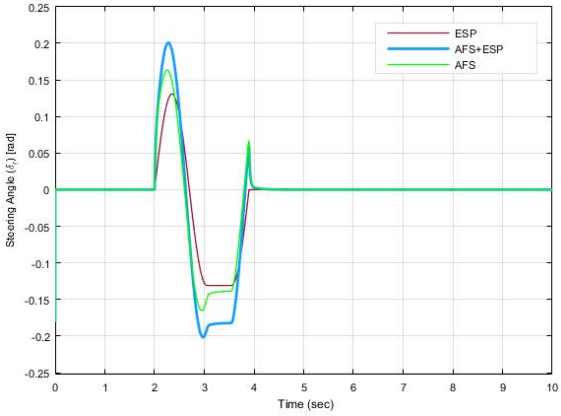

(c) Steering angle

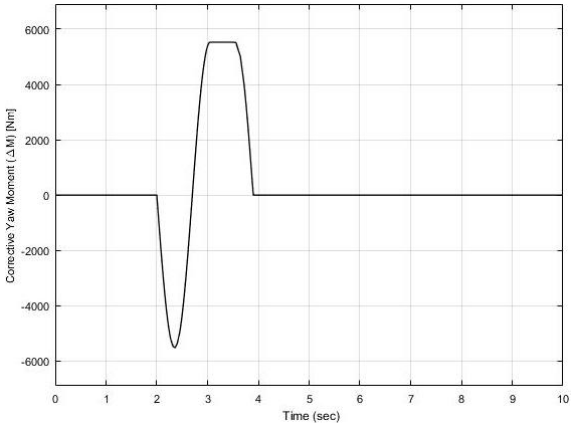

(d) Yaw moment

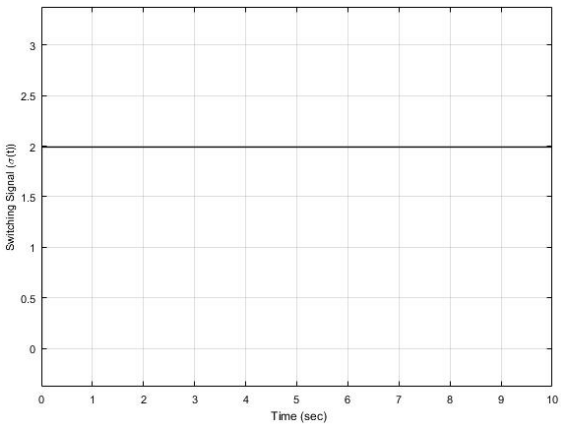

(e) Switching signal

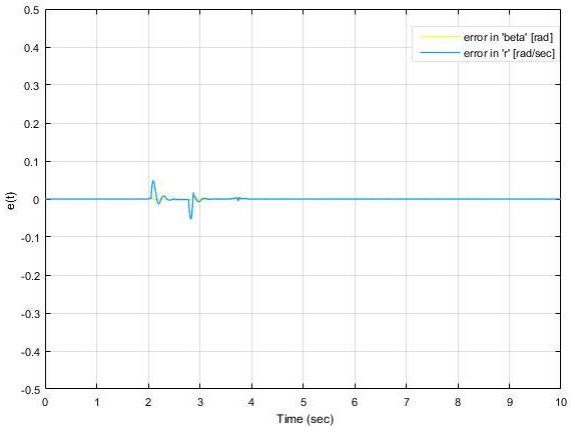

(f) Tracking error

Figure 4-10: Simulation results for SWD maneuver coasting at $15m/s$

Simulations were obtained by keeping the longitudinal velocity constant to $15m/s$. At this longitudinal velocity, the vehicle stays in the linear region. The side slip angle of the vehicle was bounded and the controller was able to track the reference yaw rate.

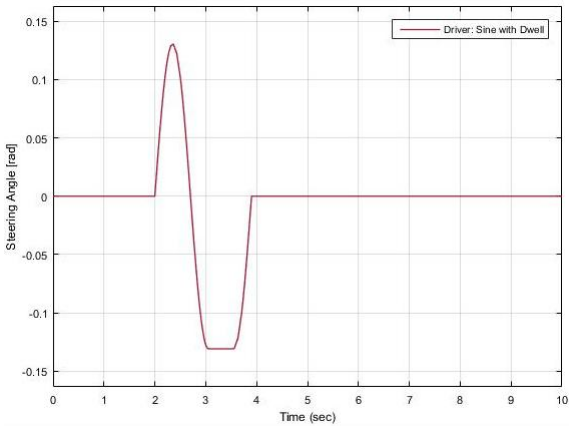

(a) Steering angle by driver

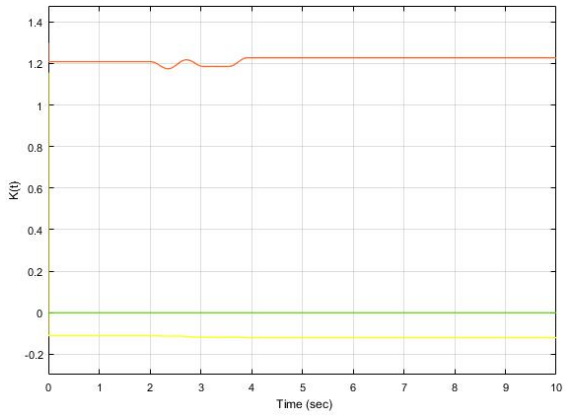

(b) Estimate of controller gain $(K(t))$

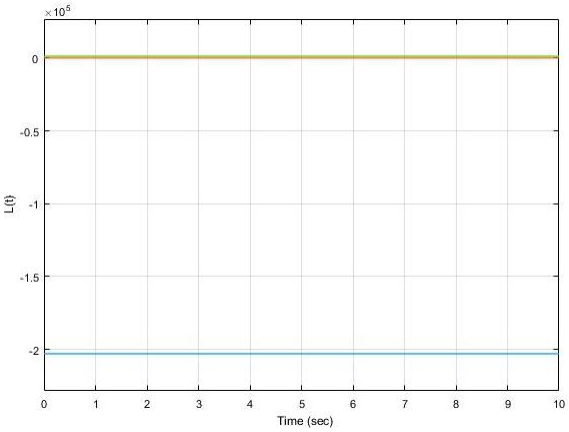

(c) Estimate of controller gain $(L(t))$

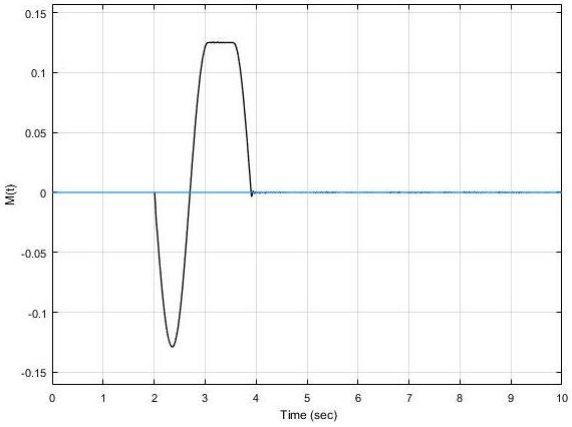

(d) Estimate of controller gain $(M(t))$

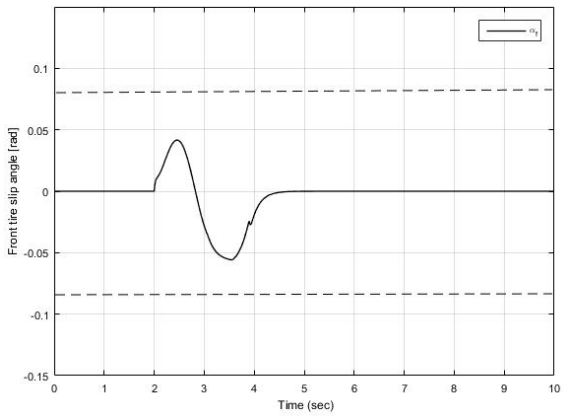

(e) Front tire slip angle (α_f)

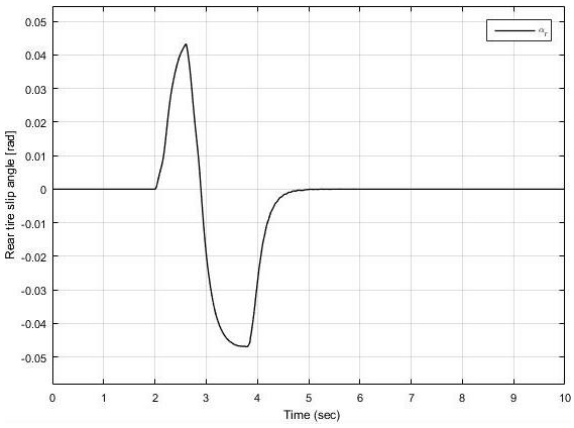

(f) Rear tire slip angle (α_r)

Figure 4-11: Simulation results for SWD maneuver coasting at $15m/s$

The slip angle of front tire saturates before the rear tire. Particularly in this case the front tire does not reach the saturation limit and vehicle dynamics remain in the linear region and switching does not occur. The switching signal was active in $Region\ 2$ for the complete simulation.

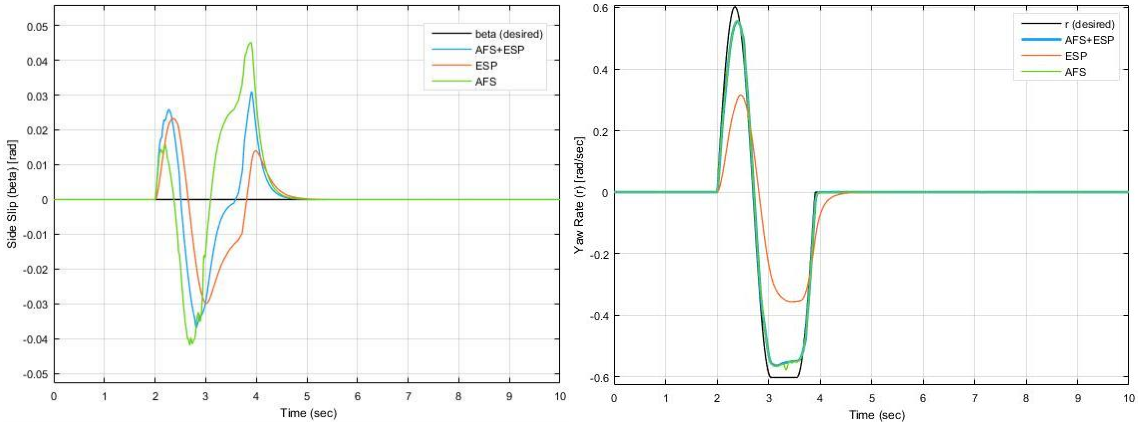

(a) Side slip angle (Linear control) **(b)** Yaw rate (Linear control)

Figure 4-12: Simulation results for SWD maneuver coasting at 15m/s with linear control only

While coasting at the constant longitudinal velocity of $15m/s$ the vehicle response were obtained in the simulations shown in Figure 4-10 to Figure 4-12. The observations made were as follows:

- The vehicle coasting at the longitudinal velocity of $15m/s$ stays in the linear region ($Region$ 2), can be seen in Figure 4-10e. The front tire slip angle (α_f) stays within the saturation limit of 0.07 rad in Figure 4-11e, which does not allow the switching to occur.
- All three control algorithms were able to ensure the lateral stability of the vehicle when the hybrid adaptive control policy was active. The side slip angle was bounded close to zero with a peak angle of 0.03 rad and yaw rate was tracking the desired trajectory smoothly with a peak of 0.6 rad/sec, and a small overshoot was observed when only ESP was working.
- The best reference tracking was obtained with the integration of the both safety systems ($AFS + ESP$) i.e when both control inputs δ_f and ΔM were active.
- The two control inputs required to stabilize the system, i.e the front tire steering angle (δ_f) and the yaw moment (ΔM) were shown in Figure 4-10c and Figure 4-10d respectively.
- As observed from Figure 4-12, the linear controller was able to give the equivalent stable response as compared to, when the hybrid adaptive controller was working. This type of response was expected as nonlinear dynamics were not excited at this particular velocity.

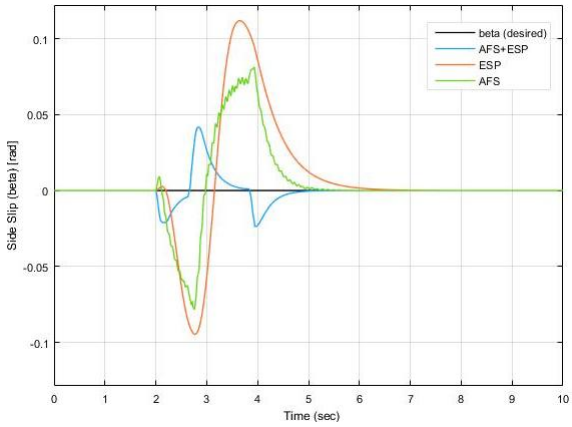

(a) Side slip angle

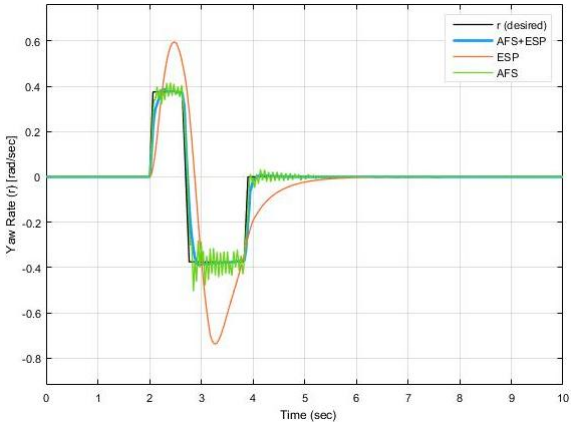

(b) Yaw rate

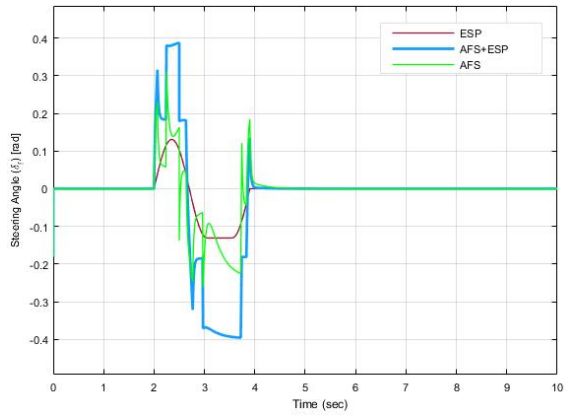

(c) Steering angle

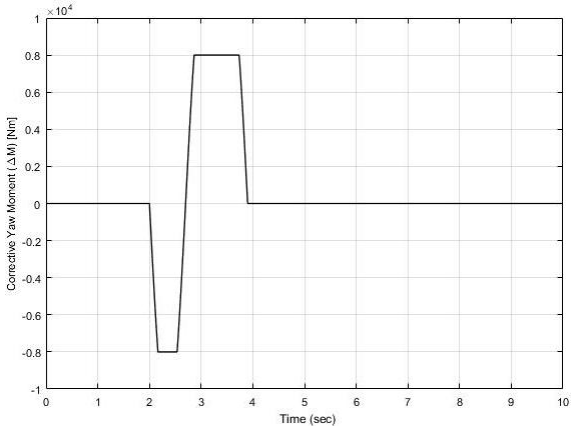

(d) Yaw moment

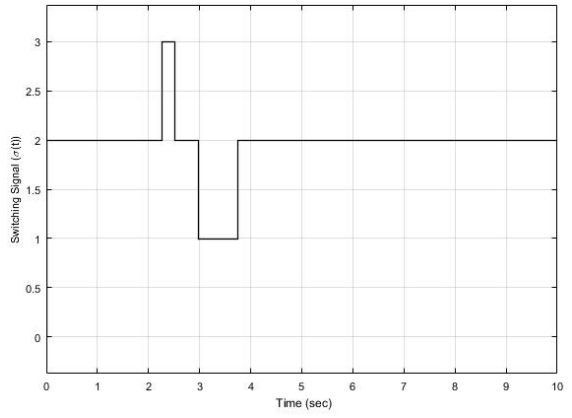

(e) Switching signal

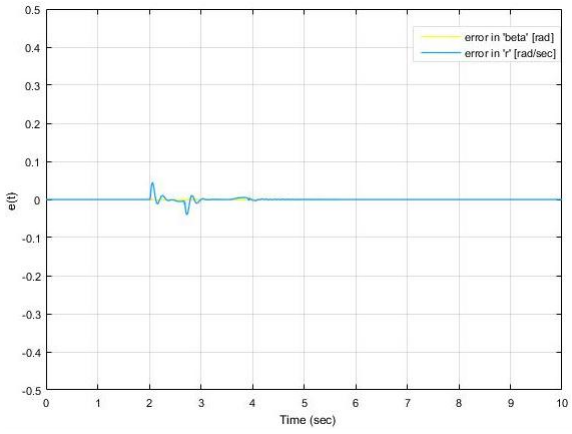

(f) Tracking error

Figure 4-13: Simulation results for SWD maneuver coasting at $20m/s$

These simulations were obtained with new tire parameters in the model and by keeping the longitudinal velocity constant to $20m/s$. This velocity pushes the vehicle towards the nonlinear behavior.

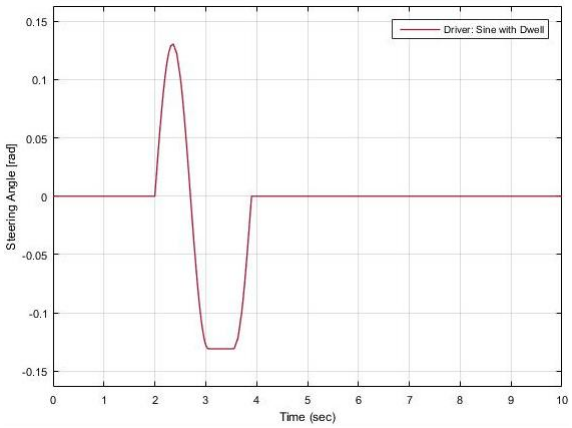

(a) Steering angle by driver

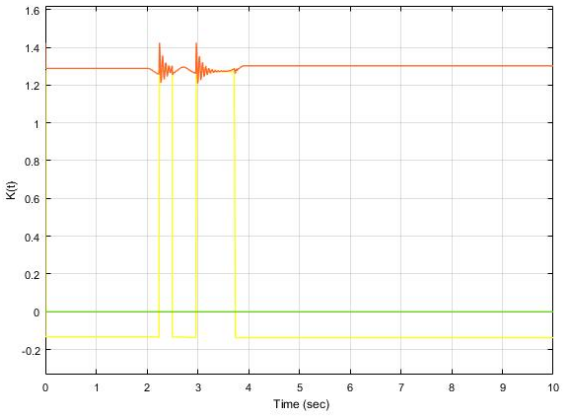

(b) Estimate of controller gain $(K(t))$

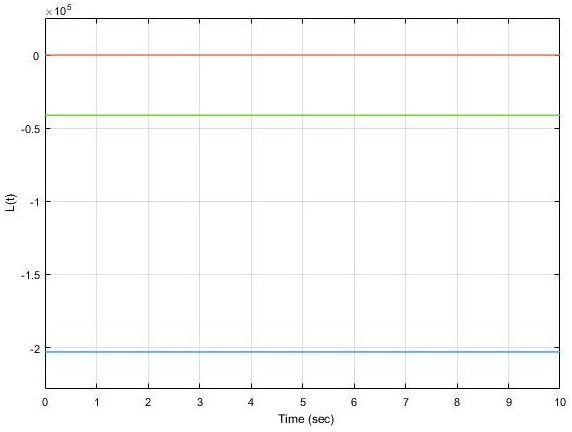

(c) Estimate of controller gain $(L(t))$

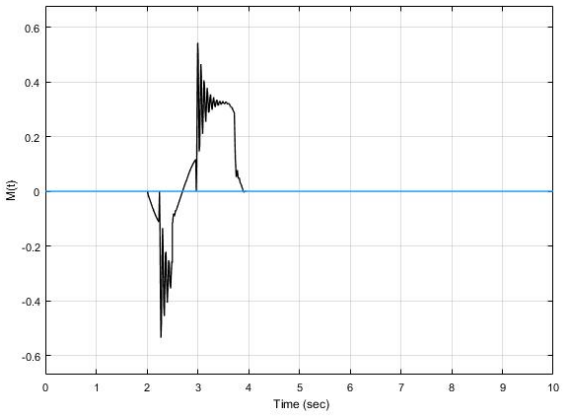

(d) Estimate of controller gain $(M(t))$

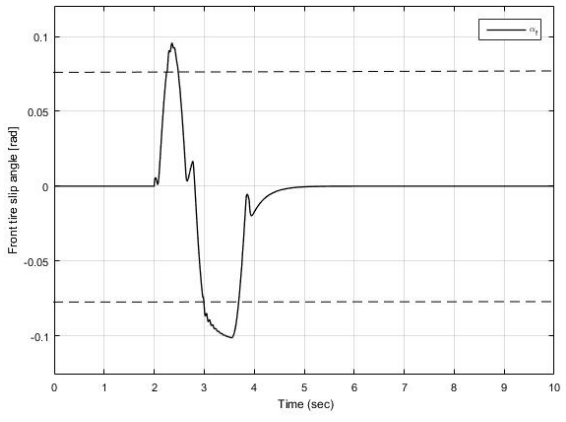

(e) Front tire slip angle (α_f)

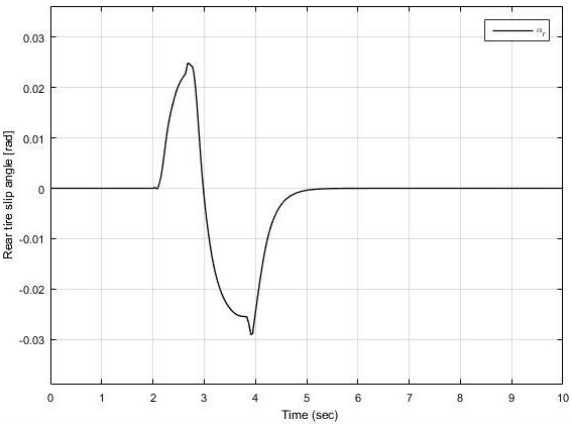

(f) Rear tire slip angle (α_r)

Figure 4-14: Simulation results for SWD maneuver coasting at $20m/s$

The slip angle of front tire saturates before the rear tire which allow the vehicle dynamics to work outside the linear region at this velocity and allows the switching to occur. With the evolution of front tire slip angle, the switching signal was active in all the three regions.

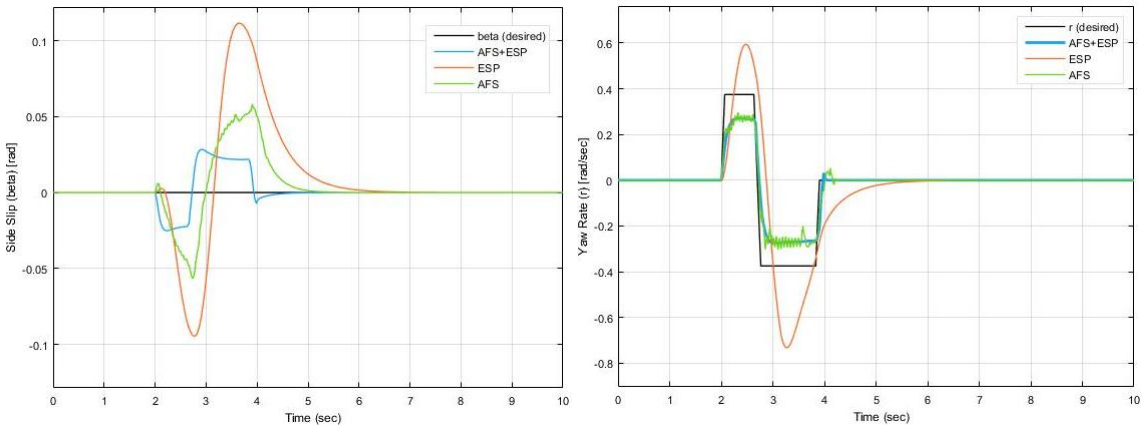

(a) Side slip angle (Linear control) **(b)** Yaw rate (Linear control)

Figure 4-15: Simulation results for SWD maneuver coasting at 20m/s with linear control only

The observations made from the Figure 4-13 to Figure 4-15 when the vehicle was coasting at constant longitudinal velocity of $20 m/s$ were as follows:

- The vehicle coasting at the longitudinal velocity of $20 m/s$ was able to excite the non-linear characteristics of the system with the new tire parameters. This can be observed by the switching signal in Figure 4-13e. The front tire slip angle (α_f) in Figure 4-14e reach the updated saturation limit of 0.07 rad for these tire parameters and allows the switching to occur.
- All three control algorithms try to achieve the lateral stability of the vehicle when the hybrid adaptive control policy was active. The ESP working alone fails to bound the side slip angle close to zero. A peak side slip angle of 0.14 rad was observed. Also, the huge overshoot of 57.89% exist in yaw rate tracking with the peak yaw rate of 0.6 rad/sec when only ESP was working.
- When only AFS was working the chattering behavior was observed in reference tracking of the yaw rate.
- Both the controller working alone were not able to provide good results. The best reference tracking was obtained with the integration of the both safety systems ($AFS + ESP$) i.e. when both control inputs δ_f and ΔM were active. It allows penalizing the large side slip angle to 0.04 rad and yaw rate to 0.385 rad/sec to prevent the vehicle from losing control.
- The two control inputs required to stabilize the system, i.e. the front tire steering angle (δ_f) and the yaw moment (ΔM) were shown in Figure 4-13c and Figure 4-13d respectively.
- The estimates of the controller parameters which allow the adaptation of the hybrid controller to follow the reference trajectory was shown in Figure 4-14.
- The norm of state tracking error can be observed in Figure 4-13f.
- As observed from Figure 4-15, with only the linear controller in action the system response became poor when compared to a working hybrid adaptive controller. The linear controller was not able to bound the side slip angle and generate the desired yaw rate required for the vehicle to safely follow the desired trajectory.

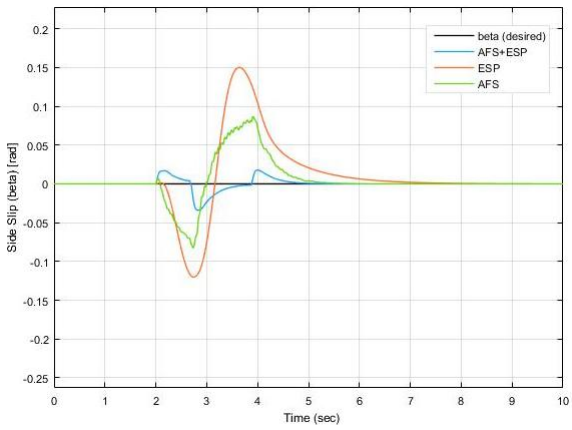

(a) Side slip angle

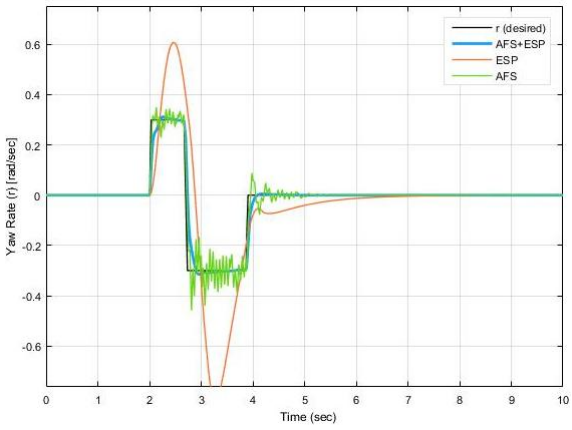

(b) Yaw rate

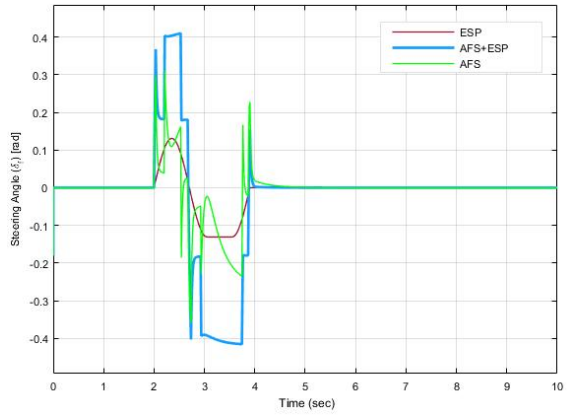

(c) Steering angle

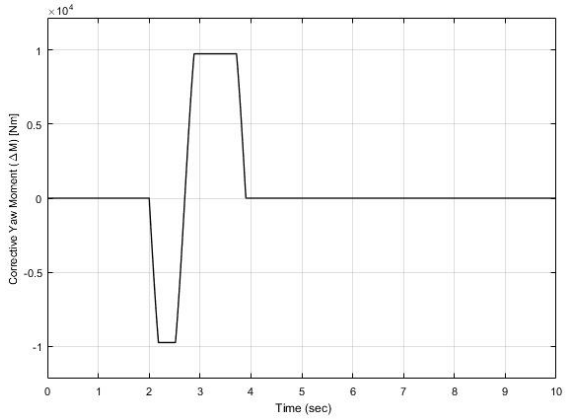

(d) Yaw moment

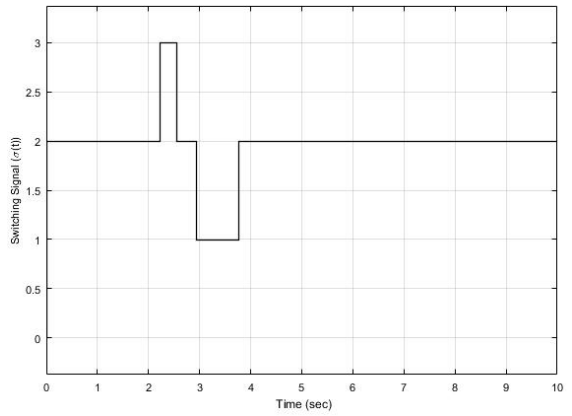

(e) Switching signal

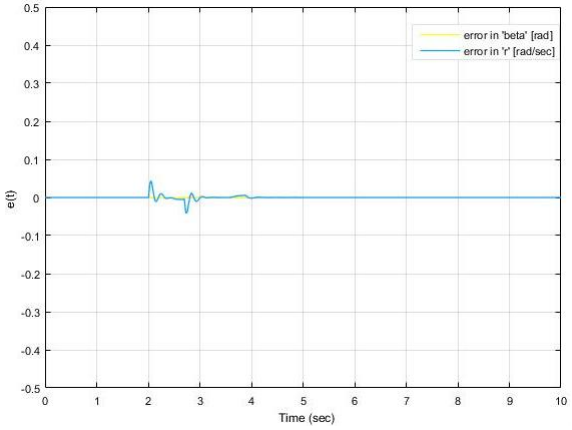

(f) Tracking error

Figure 4-16: Simulation results for SWD maneuver coasting at $25 m/s$

These simulations were obtained with new tire parameters in the model and by keeping the longitudinal velocity constant to $25 m/s$.

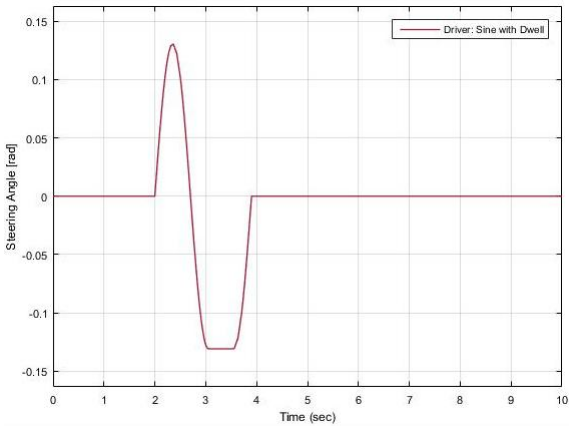

(a) Steering angle by driver

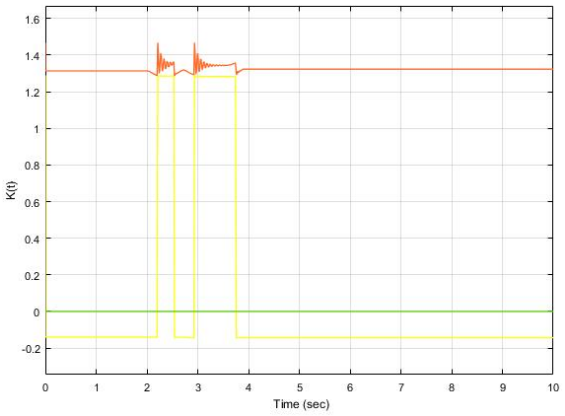

(b) Estimate of controller gain $(K(t))$

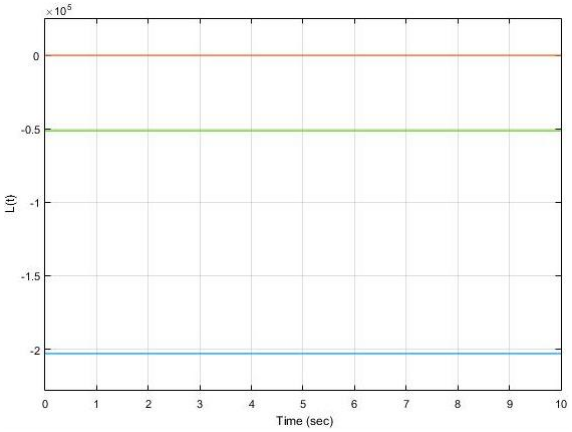

(c) Estimate of controller gain $(L(t))$

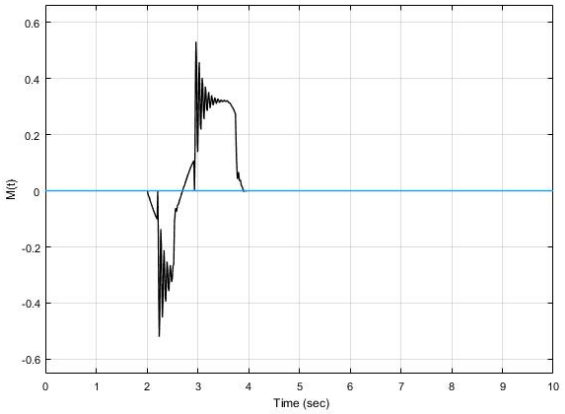

(d) Estimate of controller gain $(M(t))$

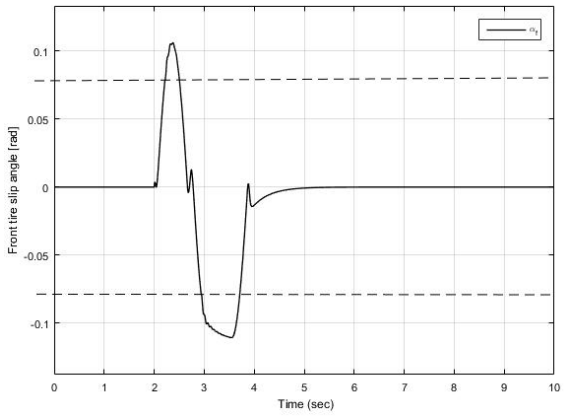

(e) Front tire slip angle (α_f)

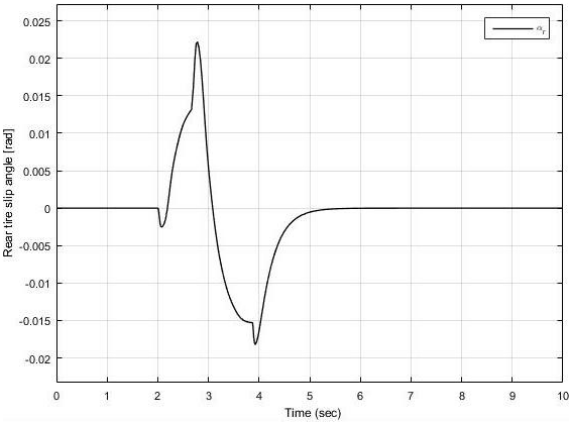

(f) Rear tire slip angle (α_r)

Figure 4-17: Simulation results for SWD maneuver coasting at $25m/s$

The slip angle of front tire saturates and allows the vehicle to work outside the linear region at this velocity. The switching occurs with the evolution of front tire slip angle and dynamics were active in all the three regions.

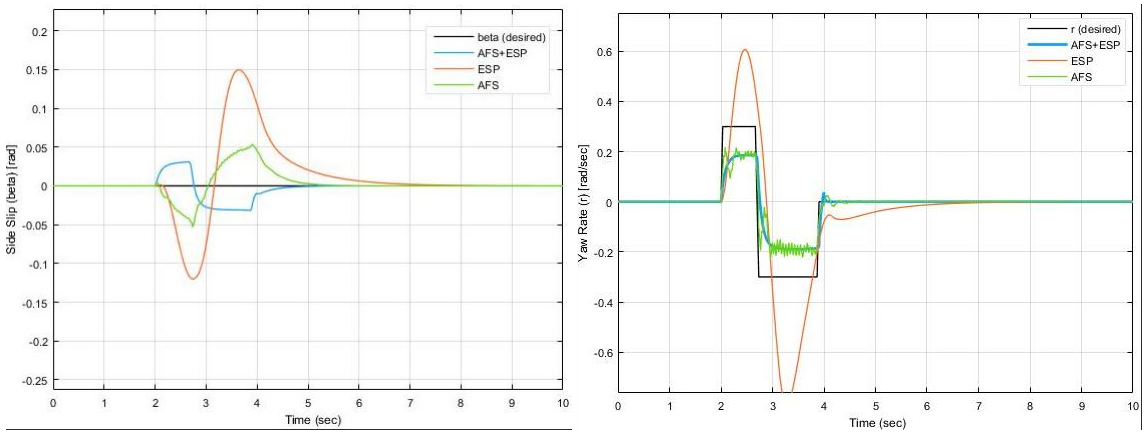

(a) Side slip angle (Linear control) **(b)** Yaw rate (Linear control)

Figure 4-18: Simulation results for SWD maneuver coasting at 25m/s with linear control only

The observations made from the Figure 4-16 to Figure 4-18 when the vehicle was coasting at constant longitudinal velocity of $25 m/s$ were as follows:

- The vehicle coasting at the longitudinal velocity of $25 m/s$ was able to excite the nonlinear characteristics of the system with the new tire parameters. This can be observed by the switching signal in Figure 4-13e. The front tire slip angle (α_f) reach the saturation limit and allows the switching to occur. This can be seen in Figure 4-17e.
- All three control algorithms try to achieve the lateral stability of the vehicle when the hybrid adaptive control policy was active. The ESP working alone fails to bound the side slip angle close to zero. A peak side slip angle of 0.15 rad was observed. Also, a huge overshoot of about 106.67% was observed in yaw rate tracking with the peak yaw rate of 0.62 rad/sec when only ESP was working.
- Both the controller working alone are not able to provide good results. The best reference tracking was obtained with the integration of the both safety systems ($AFS + ESP$) i.e. when both control inputs δ_f and ΔM were active. It allow penalizing the large side slip angle to 0.03 rad and yaw rate to 0.32 rad/sec to prevent the vehicle from losing control.
- The two control inputs required to stabilize the system, i.e. the front tire steering angle (δ_f) and the yaw moment (ΔM) were shown in Figure 4-16c and Figure 4-16d respectively.
- The estimates of the controller parameters which allow the adaptation of the hybrid controller to follow the reference trajectory were shown in Figure 4-17.
- The norm of state tracking error can be observed in Figure 4-16f.
- As observed from Figure 4-18, with only the linear controller in action the system response became poor when compared to the hybrid adaptive controller in working. The linear controller was not able to bound the side slip angle and generate the desired yaw rate required for the vehicle to safely follow the desired trajectory.

It can be observed from the three cases discussed above to check the robustness to vehicle velocity, better system performance was obtained with the hybrid adaptive policy. The lateral stability was achieved at higher velocities by compensating with the small yaw rate and relatively large side

slip angle of the vehicle. Also, the ESP stability criteria discussed in (2-15) and (2-16) were both satisfied by the hybrid adaptive control scheme and hybrid ICC passed the test. On the other hand the linear ICC failed the test based on the similar criterion. Also, it was observed that when ESP was working alone, it fails to bound the vehicle yaw rate to the desired value. The closed-loop system performance was compared in Table 4-2 and was observed that the hybrid adaptive ICC performance was best in terms of penalizing the peak overshoot in the system states. Here, the negative sign of the magnitude represents undershoot.

Table 4-2: Closed-loop system performance: Comparison

Speed ⇒	15 m/s		20 m/s		25 m/s	
Safety System ⇓	β overshoot (%)	r overshoot (%)	β overshoot (%)	r overshoot (%)	β overshoot (%)	r overshoot (%)
AFS	4.2	−8.33	7	9.09	8	40
ESP	2.4	−50	13	57.89	15	106.67
AFS + ESP	2.3	−8.33	2.5	3.89	2.5	6.67

4-3 System performance in presence of external disturbance

In this case, the performance of the controller was validated against the disturbance acting on the vehicle employed by the driver in the form of high yaw moment (generated by hard braking from hand-brakes). In this scenario just after making a steering, hard braking was also employed by the driver as the external disturbance on the vehicle. This disturbance was applied for 1 sec in between time instant $2-3$ sec. It can be observed from the system response in Figure 4-19c and Figure 4-19d that the hybrid adaptive control policy was successfully able to handle the external disturbances acting on the vehicle.

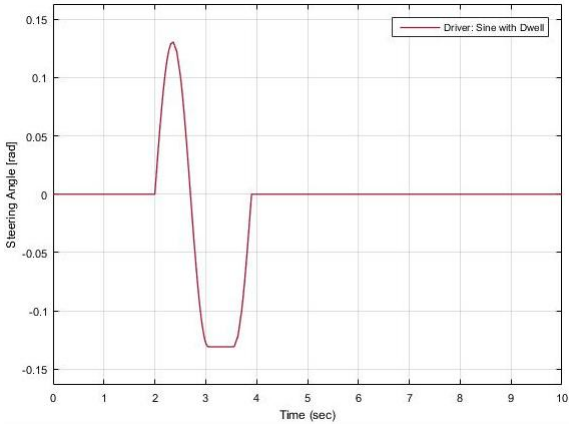

(a) Steering angle

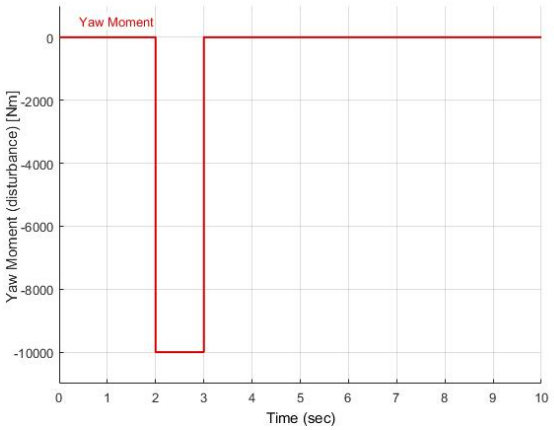

(b) Yaw moment (disturbance)

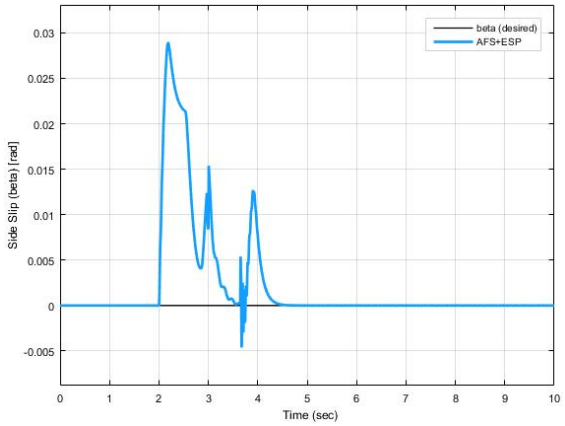

(c) Side slip angle

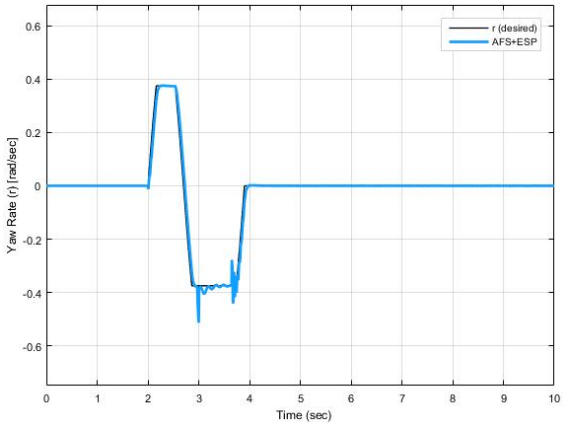

(d) Yaw rate

Figure 4-19: Simulation results for SWD maneuver coasting at $20m/s$ with external yaw moment disturbance (due to hard braking)

4-4 Controller validation

The controller which use hybrid adaptive policy was validated on the nonlinear model which was built in Simulink using the nonlinear differential equations from the 2 DOF bicycle model as described by (2-1). The parameters used in magic formula tire model were provided in Appendix A which closely match the PWA parameters used in first test case i.e the Pacejka tire parameters for high friction in between tire and road.

It was important to validate the working of the controller on the nonlinear model as in most of the practical applications we were not aware of system state space matrices A_i and B_i and it was not possible to implement the nominal control law on such type of systems. It was hence, important to check the working of the adaptive controller in this scenario.

The observations made from Figure 4-20 when the vehicle was coasting at constant longitudinal velocity of $20 m/s$ were as follows:

- The nonlinear vehicle model simulations were obtained with the longitudinal velocity kept constant at $20 m/s$. At this velocity, the switching happen with the evolution of the states of the vehicle model as seen in Figure 4-20e.
- All three control algorithms try to laterally stabilize the vehicle when the hybrid adaptive control policy was active. The side slip angle was bounded close to zero with a peak angle of 0.02 rad and yaw rate was tracking the desired trajectory with a peak of 0.385 rad/sec. The yaw tracking, in this case, was not smooth, due to the presence of the non-linearities in the system.
- The best reference tracking was obtained with the integration of the both safety systems ($AFS + ESP$) i.e when both control inputs δ_f and ΔM were active.
- The two control inputs required to stabilize the system, i.e the front tire steering angle (δ_f) and the yaw moment (ΔM) were shown in Figure 4-20e and Figure 4-20d respectively.
- The norm of state tracking error can be observed in Figure 4-20f, the error, in this case, was slightly more as compared to the similar scenario in the PWA model which ultimately tracks the zero to ensure the stability of the system.

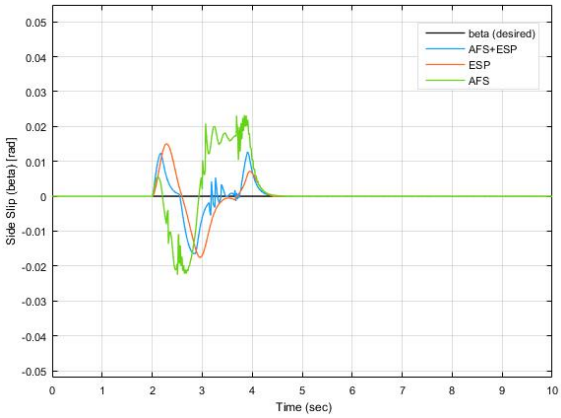

(a) Side slip angle

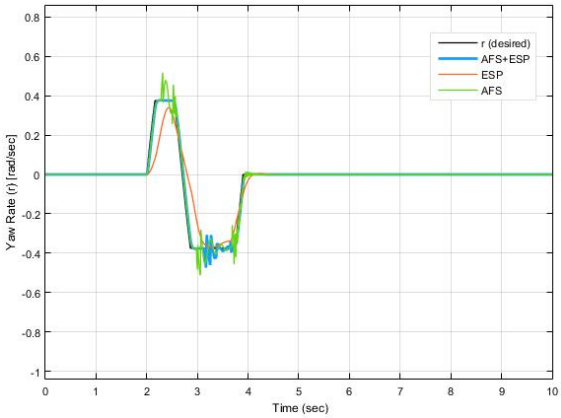

(b) Yaw rate

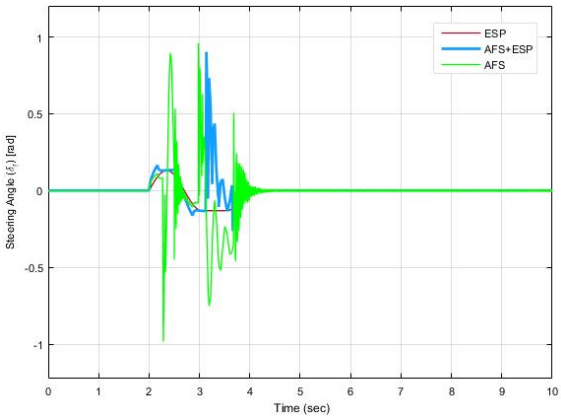

(c) Steering angle

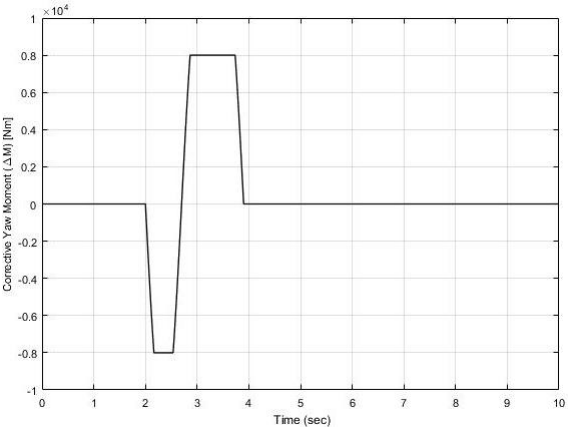

(d) Yaw moment

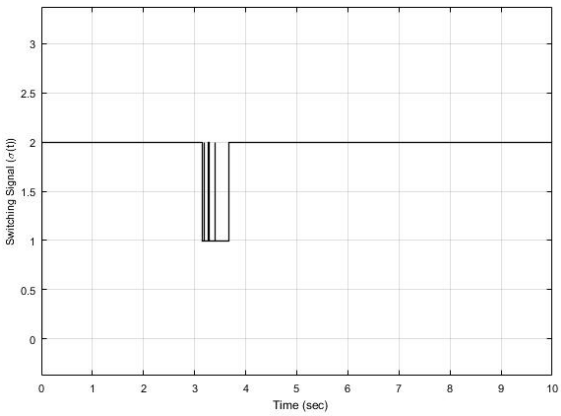

(e) Switching signal

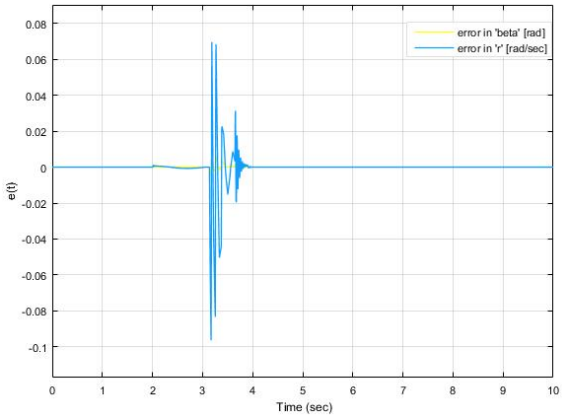

(f) Tracking error

Figure 4-20: Simulation results for SWD maneuver coasting at $20 m/s$

4-5 Summary

In this chapter, simulations were carried out on the PWA model (2-11) devised in chapter 2. The hybrid adaptive control policy was tested for its robustness against the parametric uncertainties and disturbances acting on the system. The switched ICC developed by using this design strategy was able to provide the desired stability and tracking properties, which were validated under different test conditions.

Chapter 5

Conclusion and Future Work

This chapter concludes this dissertation. In Section 5-1 the research objectives are summarized with the main contribution of this work. In Section 5-2, the new future research objectives are identified as an extension of this work.

5-1 Conclusion

The motivation to explore a novel switched ICC control scheme came up from the definition of the nonlinear vehicle model into PWA model. Current research in the field of ICC suffers from the shortcomings of the limited operating region during the controller design because of the available linearized models. This makes it difficult for the controller to give the desired performance when the driver reaches the handling limits in difficult driving maneuvers. To tackle this problem this thesis was aimed at designing a superior control technique which was able to stabilize the vehicle even when the vehicle handling limits were reached. The main contribution of this dissertation was to formulate a novel control strategy to achieve the lateral stability of a vehicle traveling in difficult driving maneuvers. Therefore, an adaptive state feedback for state tracking of a PWA system was considered. Contrary to most of the customary model reference adaptive control strategies, a piecewise affine reference model was chosen for the affine system. The adaptive control schemes were recommended, and there tracking efficiency and stability properties were evaluated.

The outcomes of the implementation procedure and simulations results lead to the following conclusions:

- The presented adaptive control scheme was able to ensure the signal boundedness and achieve the asymptotic reference tracking, such that the closed-loop system was exponentially stable and tracking errors decayed to zero.
- This control scheme could address large uncertainties in the unknown system parameters and was also robust against the disturbances employed by the driver.

- The presented switched ICC scheme was able to penalize the body side slip angle and track the reference yaw rate even when the vehicle enter its nonlinear region.
- The switched adaptive control scheme was also able to tackle uncertainties accounted in the system due to variation in speed of the vehicle and discrepancies in tire parameters.
- The proposed control scheme allowed fault tolerance operations in the presence of braking actuator failure.
- This strategy ensured stable vehicle response nearing the limits of the maneuvering capacity of the vehicle even with the 2-DOF nonlinear vehicle model.

5-2 Future work

In this dissertation the vehicle system was modeled by considering only the lateral dynamics of the vehicle but in the practical scenario this evidently will not be the case. In the realistic event, the vehicle is described in a more complex way and will include the longitudinal and vertical dynamics as well. So this thesis work can be extended with a more complex model that is able to describe the dynamics of the vehicle more closely to the actual dynamics. One of the choices for the extension of the current architecture can be done by using the CarSim model in the loop. This might require addition of new active safety systems in the integrated chassis. The possible additions could be active rear wheel steering (ARS), which can prevent the situation of oversteering to occur in the vehicle.

The current switched adaptive control architecture can also be extended to various automated vehicle scenarios like automatic lane keeping and lane changing systems, obstacle avoidance systems and platooning in order to achieve the vehicle string stability. Also, it was assumed in this research that the common boundary of two regions belongs to one of them i.e. there is no occurrence of sliding in between two regions. The current architecture can be extended to the case where the sliding can occur in the closed loop system and the assumption of being a continuous plant and reference model at the boundary is also relaxed.

A common drawback to the most of the automotive control systems is the dependence of the reference model on the coefficient of friction and slip angle. In order to overcome this issue, online estimation scheme for these variables can be integrated into the controller to analyze the performance of the controller. Also, as a future work recommendation, it should be possible to design the switched output feedback control based on yaw rate by avoiding the measurement of side slip angle of the vehicle. Since it is a tedious task to measure the tire slip angles which requires estimation algorithms and optical sensors, the partitions in the switched output feedback control can be determined based on the corresponding hyperplanes on yaw rate which can be measured cost effectively. This might provide an extension to the ongoing research in the field of vehicle stability.

Appendix A

Pacejka Magic Formula Coefficient

The tire parameters used to describe the pacejka tire model to analyze the non-linear model were provided below:

Table A-1: Pacejka magic formula coefficient: High friction road

Coefficient	Coefficient Value
B_f	6.7651
C_f	1.3000
D_f	-6436.8
E_f	-1.9990
B_r	9.0051
C_r	1.3000
D_r	-5430.0
E_r	-1.7908

Appendix B

Vehicle Model Parameters

The vehicle model parameters used to describe the PWA model were provided below:

Table B-1: Vehicle model parameters

Parameter	Description	Value	Unit
$\hat{\alpha_f}$	saturation limit (α_f)	0.101	rad
c_f	front tire cornering stiffness	$9.059 * 10^4$	N/rad
d_f	front tire PWA function coefficient	$-9.059 * 10^3$	N/rad
e_f	front tire PWA function coefficient	$1.005 * 10^4$	N/rad
c_r	rear tire cornering stiffness	$1.651 * 10^5$	N/rad
d_r	rear tire PWA function coefficient	$1.651 * 10^5$	N/rad
e_r	rear tire PWA function coefficient	0	N/rad
l_f	distance from COG to front axle	1.47	m
l_r	distance from COG to rear axle	1.43	m
m	mass of vehicle	1891	kg
I_z	yaw moment of inertia of vehicle	3213	kgm^2
v_x	longitudinal velocity	20	m/s
λ	longitudinal slip	0	

Vehicle model parameters which were used to check the robustness of the control policy against the parameter variations were updated in following table:

Table B-2: Vehicle model parameters

Parameter	Description	Value	Unit
$\hat{\alpha_f}$	saturation limit (α_f)	0.07	rad
c_f	front tire cornering stiffness	39995	N/rad
d_f	front tire PWA function coefficient	11162	N/rad
e_f	front tire PWA function coefficient	2018.3	N/rad
c_r	rear tire cornering stiffness	34993	N/rad
d_r	rear tire PWA function coefficient	34993	N/rad
e_r	rear tire PWA function coefficient	0	N/rad

Appendix C

Hybrid Adaptive Controller Design: Ideal Control Gains

While doing the initial control design the controller gains have to be specified for each particular region in order to attain the asymptotic state tracking and hence the desired performance. The nominal controller gains required in Chapter 4 were described below:

State feedback gain K_i^* obtained from LQ control:

$$K_1^* = K_3^* \begin{bmatrix} -6.2596 & -1.5358 \\ 0.0003 & 0.0001 \end{bmatrix} \qquad K_2^* = \begin{bmatrix} 0.4785 & 0.6370 \\ 0.0000 & 0.0000 \end{bmatrix}$$

Feed-forward gain L_i^* obtained from DC gain law:

$$L_1^* = L_3^* \begin{bmatrix} -23.4846 & -4.3341 \\ -4.7879 * 10^5 & -2.1362 * 10^4 \end{bmatrix} \qquad L_2^* = \begin{bmatrix} 3.3010 & 0.9976 \\ -4.7879 * 10^5 & -2.1362 * 10^4 \end{bmatrix}$$

Controller gain M_i^* obtained from Assumption 3:

$$M_1^* = M_3^* \begin{bmatrix} -1.1094 \\ 0 \end{bmatrix} \qquad M_2^* = \begin{bmatrix} 0 \\ 0 \end{bmatrix}$$

Gain S_i required for the adaptive laws were:

$$S_1 = S_3 \begin{bmatrix} 1.3576 & -0.0003 \\ -30.4293 & 0.0015 \end{bmatrix} \qquad S_2 = \begin{bmatrix} -1.0494 & 0 \\ 23.5196 & 0.0002 \end{bmatrix}$$

Bibliography

[1] S. Sadri and C. Wu, "Stability analysis of a nonlinear vehicle model in plane motion using the concept of lyapunov exponents," *Vehicle System Dynamics - International Journal of Vehicle Mechanics and Mobility*, vol. 51, no. 6, pp. 906–924, March 2013.

[2] J. Wong, *Theory of Ground Vehicles 3rd ed.* John Wiley & Sons, 2001.

[3] H. B. Pacejka, *Tyre and Vehicle Dynamics*. Butterworth-Heinemann, 2012.

[4] *Lecture Slides Vehicle Dynamics B (ME41115)*. Delft University of Technology, 3mE.

[5] D. Liberzon, *Switching in Systems and Control*. Springer Science & Business Media,Birkhauser, Boston, 2003.

[6] M. D. Bernardo, U. Montanaro, and S. Santini, "Novel switched model reference adaptive control for continuous piecewise affine systems," *Proceedings of the* 47^{th} *IEEE Conference on Decision and Control Cancun, Mexico*, Dec. 9-11, 2008.

[7] T. Gordan, M. Howell, and F. Brandao, "Integrated control methodologies for road vehicle," *Vehicle System Dynamics*, vol. 40, no. 1-3, 2003.

[8] R. Rajamani, *Vehicle Dynamics and Control*. Springer, second edition.

[9] M. Nagai, M. Shino, and F. Gao, "Study on integrated control of active front steer angle and direct yaw moment," *JSAE review*, vol. 23, no. 3, p. 309–315, 2002.

[10] S. S. You and S. K. Jeong, "Controller design and analysis of automatic steering of passenger cars," *Mechatronics*, vol. 12.

[11] E. Ono, S. Hosoe, H. D. Tuan, and S. ichi Doi, "Bifurcation in vehicle dynamics and robust front wheel steering control," *IEEE Transactions on control systems technology*, vol. 6, no. 3, pp. 412–420, May 1998.

[12] T. Shim, S. Chang, and S. Lee, "Investigation of sliding surface design on the performance of sliding mode controller in anti-lock braking systems," *IEEE Transactions on Vehicular Technology*, vol. 57, no. 2, p. 747–759, 2008.

[13] M. A. Arat, K. B. Singh, and S. Taheri, "An intelligent tyre based adaptive vehicle stability controller," *International Journal of vehicle design*, vol. 65, no. 2-3, 2014.

[14] T. Fukao, S. Miyasaka, K. Mori, N. Adachi, and K. Osuka, "Active steering systems based on model reference adaptive nonlinear control," *IEEE Intelligent Transportation Systems Conference Proceedings*, August 2001.

[15] N. Ding and S. Taheri, "An adaptive integrated algorithm for active front steering and direct yaw moment control based on direct lyapunov method," *Vehicle System Dynamics*.

[16] P. Falcone, H. E. Tseng, F. B. an J. Asgari, and D. Hrovat, "Mpc-based yaw and lateral stabilisation via active front steering and braking," *Vehicle System Dynamics, Taylor and Francis*, 28 Jan 2009.

[17] J. Tjonnas and T. A. Johansen, "Adaptive optimizing dynamic control allocation algorithm for yaw stabilization of an automotive vehicle using brakes,"

[18] F. Tahami, S. Farhangi, and R. Kazemi, "A fuzzy logic direct yaw-moment control system for all-wheel-drive electric vehicles," *Vehicle System Dynamics*, vol. 41, no. 3, pp. 203–221, 2004.

[19] D. Bernardini, S. D. Cairano, A. Bemporad, and H. Tseng, "Drive-by-wire vehicle stabilization and yaw regulation: a hybrid model predictive control design," *Joint 48^{th} IEEE Conference on Decision and Control and 28^{th} Chinese Control Conference Shanghai, P.R. China,*, Dec 16-18 2009.

[20] I. Stefano Di Cairano, Member, H. E. Tseng, D. Bernardini, and I. Alberto Bemporad, Fellow, "Vehicle yaw stability control by coordinated active front steering and differential braking in the tire sideslip angles domain," *IEEE Transactions on Control Systems Technology*, vol. 21, no. 4, 4,July,2013.

[21] S. Scalzi, A. Benine-Neto, M. Netto, W. Pasillas-Lepine, and S. Mammar, "Active steering control based on piecewise affine regions," *2010 American Control Conference, Marriott Waterfront, Baltimore, MD, USA*, June 30-July 02, 2010.

[22] A. Benine-Neto and S. Mammar, "Piecewise affine state feedback controller for lane departure avoidance," *2011 IEEE Intelligent Vehicles Symposium (IV), Baden-Baden, Germany*, June 5-9, 2011.

[23] G. Palmieri, M. Baric, L. Glielmo, E. H. Tseng, and F. Borrelli, "Robust vehicle lateral stabilization via set-based methods for uncertain piecewise affine systems: Experimental results," *2011* 50^{th} *IEEE Conference on Decision and Control and European Control Conference (CDC-ECC) Orlando, FL, USA*, December 12-15, 2011.

[24] A. Benine-Neto and C. Grand, "Piecewise affine control for fast unmanned ground vehicles," *2012 IEEE/RSJ International Conference on Intelligent Robots and Systems, Vilamoura, Algarve, Portugal*, October 7-12, 2012.

[25] M. D. Bernardo, U. Montanaro, and S. Santini, "Minimal control synthesis adaptive control of continuous bimodal piecewise affine system," *SIAM Journal on Control and Optimization*, vol. 48, no. 7, pp. 4242–4261, 2010.

[26] M. D. Bernardo, U. Montanaro, and S. Santini, "Hybrid model reference adaptive control of piecewise affine systems," *IEEE Transactions on Automatic Control*, vol. 58, no. 2, pp. 304–316, 2013.

[27] G. Liu, H. Ren, S. Chen, and W. Wang, "The 3-dof bicycle model with the simplified piecewise linear tire model," *2013 International Conference on Mechatronic Science, Electrical Engineering and Computer, Shenyang, China*, Dec 20-22 2013.

[28] A. Benine-Neto, S. Scalzi, M. Netto, S. Mammar, and W. Pasillas-Lepine, "Vehicle yaw rate control based on piecewise-affine regions," *2010 IEEE Intelligent Vehicle Symposium, University of California, San Diego, CA, USA*, June 21-24 2010.

[29] E. Ono, S. Hosoe, H. D. Tuan, and S. ichi Doi, "Bifurcation in vehicle dynamics and robust front wheel steering control," *IEEE Transactions on control systems technology*, vol. 6, no. 3, pp. 412–420, May 1998.

[30] A. Benine-Neto and C. Grand, "Piecewise affine control for fast unmanned ground vehicles," *2012 IEEE/RSJ International Conference on Intelligent Robots and Systems*, pp. 3673–3678, October 7-12, 2012.

[31] S. Shen, J. Wang, P. Shi, and G. Premier, "Nonlinear dynamics and stability analysis of vehicle plane motions," *Vehicle System Dynamics*, vol. 45, no. 1, pp. 15–35, Jan 2007.

[32] N. A. et al., "Proposed fmvss no. 126 electronic stability control systems," *US Department of Transportation, Washington D.C*, 2006.

[33] Q. Sang and G. Tao, "Multivariable adaptive piecewise linear control design for nasa generic transport model," *Journal of Guidance, Control, and Dynamics*, vol. 35, no. 5, pp. 1559–1567, 2012.

[34] J. Hespanha and A. Morse, "Stability of switched systems with average dwell time," *Electrical Engineering Department, University of Southern California, Technical Report*, 1999.

[35] D. Liberzon and A. Morse, "Basic problem in stability and design of switched system," *IEEE Control Systems*, vol. 19, no. 5, pp. 59–70, 1999.

[36] Q. Sang and G. Tao, "Adaptive control of piecewise linear system: The state tracking case," *IEEE transactions on Automatic Control Systems*, vol. 57, no. 2, pp. 522–528, 2012.

[37] G. Tao., *Adaptive control design and analysis.* John Wiley & Sons, 2003.

[38] G. Tao., *Multivariable adaptive control: A survey.* Automatica, (11):2737–2764, 2014.

[39] R. N. Shorten and K. S. Narendra, "On the stability and existence of common lyapunov functions for stable linear switching systems," *Proceedings of the* 37^{th} *IEEE Conference on Decision and Control Tampa, Florida USA*, pp. 3723–3724, 1998.

Glossary

List of Abbreviations

ABS	Anti-lock Braking System
ADAS	Advanced Driving Assisting System
AFS	Active Front Steering
CA	Control Allocation
COG	Center of Gravity
DOF	Degree of Freedom
DYC	Dynamic Yaw Control
ESP	Electronic Stability Program
FMVSS	Federal Motor Vehicle Safety Standards
ICC	Integrated Chassis Control
LMI	Linear Matrix Inequality
LQR	Linear Quadratic Regulator
MPC	Model Predictive Control
MRAC	Model Reference Adaptive Control
PWA	Piecewise Affine
SWD	Sine with Dwell

Nomenclature

α	tire slip angle
α_f, α_r	front and rear tire slip angle
β	side slip angle of vehicle
$\chi(t)$	indicator functions
ΔM	corrective yaw moment
Δ_{A_m}	largest difference between reference model state matrices
δ_f	front tire steering angle
$\dot{\beta}$	rate of change of side slip angle
$\dot{r}$	yaw acceleration
$\hat{\alpha_f}$	saturation value of front tire slip angle
$\lambda_{\max}[.], \lambda_{\min}[.]$	maximum and minimum eigenvalues of a square matrix
$\mathbb{N}$	set of natural numbers
$\mathbb{R}$	set of real numbers
$\mathscr{L}_2$	class of vector signal $x \in \mathbb{R}^n$ such that $\sqrt{x^T(t)x(t)} < \infty$, $\forall\, t \geq 0$;
Ω	system operating region of interest
A_i, B_i, f_i	system parameter matrices of the i^{th} system mode
a_{mi}, λ_{mi}	positive constants
A_{mi}, B_{mi}, f_{mi}	reference model system parameter matrices of the i^{th} system mode
a_y	lateral acceleration
$e(t)$	state tracking error vector
F_f, F_r	lateral force on front and rear tires respectively
I_z	yaw inertia
l_f, l_r	distance of front and rear axle from COG of vehicle
m	vehicle mass
M_z	self aligning torque
P_{mi}, Q_{mi}	symmetric, positive definite matrices satisfying lyapunov stability

r	yaw rate
S_i	known square matrix indicating control direction
T_0	minimum duration between consecutive mode switches
$u(t)$	system control input vector with respect to i^{th} system mode
v_x, v_y	longitudinal and lateral vehicle velocity
$x(t)$	system state vector with respect to i^{th} system mode
$x_{mi}(t), r(t)$	reference model system state and input vector for the i^{th} system mode